Little By Little: Continual Learning via Incremental Mixture of Rank-1 Associative Memory Experts

Anonymous Authors[1]

Abstract

Continual learning (CL) with large pre-trained models is challenged by task interference and catastrophic forgetting. Existing LoRA-based Mixture-of-Experts (MoE) methods mitigate forgetting by adding new task-specific adapters and freezing old ones, but often suffer from redundancy, interference, and ambiguous routing due to *coarse-grained* experts and routing. Coarse-grained experts (*i.e.*, full LoRA adapters with large rank) encode low-specialty information. Newly added experts often duplicate or conflict with existing ones, causing redundancy and interference. Their low specialization further confuses the router, accelerating routing degradation and forgetting as experts accumulate. In this work, we propose **MoRAM** (**M**ixture **o**f **R**ank-1 **A**ssociative **M**emory). Grounded in the view that weight matrices function as linear associative memories, MoRAM achieves CL as gradual incrementing of **atomic rank-1 memory experts**. Each rank-1 adapter acts as a fine-grained MoE expert or an associative memory unit. By viewing rank-1 adapters as key–value pairs, we eliminate explicit routers in MoE-LoRA, using a self-activation mechanism where each memory atom evaluates its own relevance via its intrinsic key. This transforms the adaptation process into robust, content-addressable retrieval. Extensive experiments on CLIP and LLMs demonstrate that MoRAM significantly outperforms state-of-the-art baselines, achieving superior plasticity-stability trade-offs, improving generalization while mitigating forgetting.

"Little by little, we gave you everything you ever dreamed of ..." — "Little by little", Oasis.

[1]Anonymous Institution, Anonymous City, Anonymous Region, Anonymous Country. Correspondence to: Anonymous Author <anon.email@domain.com>.

Preliminary work. Under review by the International Conference on Machine Learning (ICML). Do not distribute.

1. Introduction

Continual learning (CL) (Hadsell et al., 2020; De Lange et al., 2021; Ding et al., 2022) aims to enable models to incrementally and efficiently acquire new knowledge from a stream of tasks, without catastrophic forgetting (Nguyen et al., 2019; McCloskey & Cohen, 1989) or the need for repeated fine-tuning on all previously seen data (Wang et al., 2022f; 2024). With the ascendancy of Large Pre-trained Models (PTMs) in vision (Dosovitskiy et al., 2020; Radford et al., 2021) and language (Raffel et al., 2020; Grattafiori et al., 2024), the challenge has shifted: *how do we efficiently insert specific new capabilities into a massive, static memory structure without disrupting its existing generalized knowledge?*

A dominant approach for adapting PTMs is Parameter-Efficient Fine-Tuning (PEFT), particularly Low-Rank Adaptation (LoRA, Fig. 1(a)) (Hu et al., 2021). While efficient, standard LoRA applies updates as "dense" modifications to the weight space. This creates a fundamental conflict: to learn a new task, the model must inevitably alter the representation space used by previous tasks, leading to interference and forgetting (Biderman et al., 2024). To mitigate this, recent works have adopted Mixture-of-Experts MoE frameworks using LoRA adapters as experts (Fig. 1(b)) have been studied (Dou et al., 2023; Wu et al., 2024b) and have been widely adopted in CL (Yu et al., 2024; Wang et al., 2024; Yang et al., 2024; Chen et al., 2024; Li et al., 2025). These works either predefine an MoE with LoRA for CL (Yang et al., 2024), or incrementally add experts (Wang et al., 2024) or task-specific routers (Yu et al., 2024), assuming MoE benefits CL by isolating task interference. Such methods (Wang et al., 2024; Qiao & Mahdavi, 2024; Rusu et al., 2016; Yu et al., 2024) freeze old components and add new ones (e.g., experts or routers) to reduce forgetting. Despite design differences, we collectively refer a plain and general design with LoRA-based MoE as MoE-LoRA. In MoE-LoRA models, each expert is a LoRA adapter with multiple ranks (in subspaces), and the router selects among experts with each LoRA adapter as a unit.

However, current MoE-LoRA approaches operate at a *coarse granularity* that limits their effectiveness in CL. Treating entire rank-r adapters as indivisible experts forces

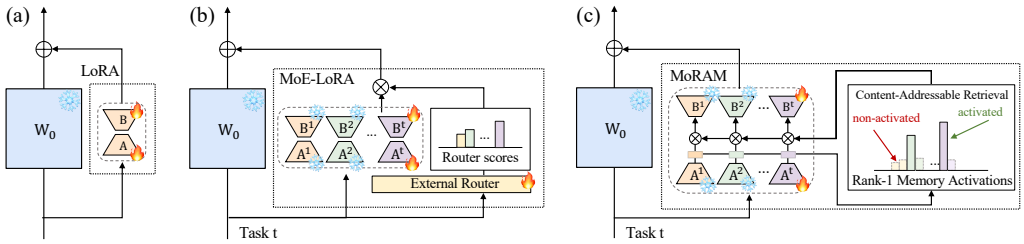

Figure 1. Conceptual illustration of CL with (a) LoRA, (b) MoE-LoRA, and (c) MoRAM (Ours).

each coarse-grained expert to be activated and learned as a single unit. It makes each expert to learn a broad range of information, leading to low specialty and combinatorial expressivity (He, 2024; Ludziejewski et al., 2024; Dai et al., 2024). It specifically introduce three challenges:

(1) Interference: A coarse expert contains a mix of low-specialty knowledge. Activating coarse-grained experts (*i.e.*, LoRA adapters with large rank) for a specific input inevitably triggers irrelevant subspaces, causing interference.

(2) Redundancy: New experts cannot selectively reuse specific "atoms" of knowledge from old experts; if the limited combination cannot cover the new task, they must relearn entire blocks, leading to inefficient capacity usage.

(3) Routing/Retrieval Collapse: The low-specialization of coarse-grained experts further confuse the router. As the number of experts grows, routers increasingly struggle to reliably index the expanding expert pool ("routing ambiguity"), leading to routing collapse and drift of old experts, and ultimately accelerating forgetting.

The coarse-grained experts and these resulted challenges limit the potential of promising MoE-LoRA design.

To address the limitations, we fundamentally rethink adaptation by synthesizing the intrinsic dimensionality of PTMs (Aghajanyan et al., 2020) through the lens of Linear Associative Memory (Kohonen, 1972). While PTMs reside in a high-dimensional parameter space, they operate on a low-rank manifold, effectively functioning as a composition of atomic key-value pairs of a memory system (Kohonen, 1972). From this perspective, the optimal CL update is not a "dense matrix" or "coarse adapters", but an associative memory system with expandable and retrievable atomic memory units. Conventional methods that update entire matrices of PTM inevitably alter the global interference patterns of the memory, easily causing catastrophic forgetting. Coarse-grained MoE-LoRA methods suffer from brittle expert expansion and retrieval. From a memory-augmentation perspective, we treat CL as incremental external memory expansion with fine-grained atomic memory units for specialization and efficiency, while casting inference as input-specific memory retrieval and application.

Based on this insight, we propose **MoRAM** (**M**ixture **o**f **R**ank-1 **A**ssociative **M**emory), a framework that continually updates PTMs by incrementing an associative memory system with atomic rank-1 experts "little by little" (Fig. 1(c)). The associative memory can also be seen as a mixture-of-expert model with rank-1 adapters as experts. Each rank-1 adapter acts as a fine-grained MoE expert or an atomic memory unit. By viewing rank-1 expert as key–value memory pairs, we can naturally eliminate the additional explicit routers in MoE-LoRA. With the proposed self-activation mechanism, each expert can evaluate its own relevance to the input via its intrinsic key. This shifts the paradigm from *address-based routing* (learning where to send data) to *content-addressable retrieval* (inputs automatically triggering the correct memory). This operation eliminates the source of routing collapse and forgetting from the additional router, increasing reliability of the memory retrieval, even as memory bank expands, while reducing computation.

Our contributions are as follows: (1) We introduce MoRAM, a novel CL framework that treats Rank-1 updates as atomic associative memory experts, enabling fine-grained knowledge reuse and minimizing interference. (2) We propose a sparse self-activation routing mechanism that eliminates external routers, allowing the model to sparsely retrieve relevant memory atoms based on input content alone. (3) We conduct extensive evaluations on both vision–language (CLIP) and large language model (LLM) benchmarks. Empirical results demonstrate that MoRAM significantly outperforms state-of-the-art methods, achieving superior plasticity-stability trade-offs, while effectively preserving pre-trained generalization capabilities.

2. Related Work

Continual learning enables sequential knowledge acquisition without forgetting. Experience replay (ER) methods (Luo et al., 2023; Aljundi et al., 2019b; Chaudhry et al., 2018a; Liu et al., 2020; Chaudhry et al., 2018b; Yan et al., 2022; 2021) interleave past examples with new data. Parameter regularization (Kirkpatrick et al., 2017; Aljundi et al., 2018; Zenke et al., 2017; Aljundi et al., 2019a; Jha et al., 2023) penalizes updates to critical weights. Dynamic networks (Zhou et al., 2024; Wang et al., 2022a;b; Zhou et al.,

2022; Wang et al., 2024; McDonnell et al., 2024; Liang & Li, 2024; Wang et al., 2022f;e; Smith et al., 2023; Wang et al., 2022c; 2024) allocate new capacity on the fly and preserve dedicated pathways for prior tasks.

Continual learning of PTMs. For CL on vision–language CLIP model (Jha et al., 2024; Zhang et al., 2024b; Garg et al., 2023), methods like ZSCL (Zheng et al., 2023) retain zero-shot performance during adaptation, and follow-up work (Yu et al., 2024; Tang et al., 2025; Xu et al., 2024; Lu et al., 2024; Wu et al., 2025) continually fine-tunes while leveraging frozen pre-trained predictions. The X-TAIL benchmark (Xu et al., 2024) further challenges models by mixing domain labels at test time. In language models (LMs) (de Masson D'Autume et al., 2019; Qin & Joty, 2021; Razdaibiedina et al., 2023; Wang et al., 2023a; Qiao & Mahdavi, 2024), continual learning uses capacity expansion or task-specific submodules to reduce interference.

Low-rank adaptation (LoRA) (Hu et al., 2021) is widely used for parameter-efficient fine-tuning of large pre-trained models. Building on this foundation, recent methods have reformulated LoRA's updates via SVD-based initialization and dynamic rank scheduling (Zhang et al., 2024a; Meng et al., 2024; Ding et al., 2023; Zhang et al., 2023; Liu et al., 2024; Wu et al., 2024a), demonstrating that task adaptation primarily relies on finding a compact subspace. In this work, we offer a complementary perspective by treating both the pre-trained weight matrix and its low-rank updates through the lens of linear associative memory (Li et al., 2018; Aghajanyan et al., 2020; Kohonen, 1972; Anderson, 1972). Under this formulation, a rank-r update corresponds to r new memory entries into the matrix, where each rank-1 component is an atomic memory slot.

Mixture-of-Experts (MoE) with LoRA. MoE scales capacity by routing inputs to sparse expert subnetworks via load-balancing (Shazeer et al., 2017; Lepikhin et al., 2020; Fedus et al., 2022; Dai et al., 2024). This paradigm has been adapted for LoRA fine-tuning (Chen et al., 2023; Li et al., 2024; Dou et al., 2023) and CL (Yu et al., 2024; Wang et al., 2024; Yang et al., 2024; Chen et al., 2024) by treating adapters as experts, typically frozen per task to prevent forgetting. In contrast, we decompose rank-r updates into r atomic rank-1 components and compute an input-dependent mixture over these fine-grained experts, significantly enhancing specialization and diversity.

3. Methods

3.1. Preliminaries

Continual learning. In CL, a model sequentially learns T tasks. For task $t \in 1, \ldots, T$, let $\mathcal{D}^t = \{(\mathbf{x}_i^t, y_i^t)\}_{i=1}^{N^t}$, where $\mathbf{x}_i^t \in \mathbb{R}^{n \times d}$, $y_i^t \in \mathcal{C}^t$, and N^t is the number of examples. In the memory-free setting, the model may access only $\mathcal{D}^t$ and cannot access data from any $\mathcal{D}^u$ with $u < t$.

Low-rank adaptation. LoRA (Hu et al., 2021) parameterizes a low-rank update to a pre-trained weight matrix $\mathbf{W}_0 \in \mathbb{R}^{d_{\text{out}} \times d_{\text{in}}}$ by introducing two factors $\mathbf{B} \in \mathbb{R}^{d_{\text{out}} \times r}$ and $\mathbf{A} \in \mathbb{R}^{r \times d_{\text{in}}}$, such that $\Delta\mathbf{W} = \mathbf{BA}$, where $r \ll \min(d_{\text{in}}, d_{\text{out}})$. The updated weight matrix is then defined as:

$$\mathbf{W} = \mathbf{W}_0 + \Delta\mathbf{W} = \mathbf{W}_0 + \mathbf{BA}. \tag{1}$$

In this formulation, the original weights $\mathbf{W}_0$ remain fixed, and only $\mathbf{B}$ and $\mathbf{A}$ are trained, reducing the number of trainable parameters from $d_{\text{in}} d_{\text{out}}$ to $r(d_{\text{in}} + d_{\text{out}})$. While parameter-efficient, standard LoRA applies the rank-r update densely to every input. This would result in updates for a new task inevitably perturb the subspaces used by prior tasks, leading to interference.

Mixture-of-Experts LoRA. Building on the Mixture-of-Experts (MoE) paradigm, a common generic framework of MoE-LoRA (Yu et al., 2024; Wang et al., 2024) treats each LoRA as an independent expert. Suppose after T tasks, we have T LoRA experts $\{(\mathbf{A}^1, \mathbf{B}^1), \ldots, (\mathbf{A}^T, \mathbf{B}^T)\}$. For an input token $x \in \mathbb{R}^{d_{\text{in}}}$, the overall LoRA update in this framework is given by $\Delta\mathbf{W} = \sum_{i=1}^{T} R(x)_i \mathbf{B}^i \mathbf{A}^i$, where the mixture weight $R(x) \in \mathbb{R}^T$ is produced by a learned router $R(\cdot) = \text{softmax}(x\mathbf{W}_r)$ and $\mathbf{W}_r \in \mathbb{R}^{d_{\text{in}} \times T}$ contains the router's trainable parameters. Each LoRA's contribution is weighted by the learnable router, enabling the model to dynamically select and combine the most relevant low-rank updates for each token. In practice, a `top-k` masking is typically applied to mixture weights to enforce sparsity, activating only the k most relevant experts. However, this design remains coarse-grained. Each expert is a dense rank-r block, and the external router $R(\mathbf{x})$ must learn to map inputs to these overlapping experts. As the number of tasks grows, this external mapping becomes ambiguous, leading to routing collapse and forgetting.

3.2. Weights as Linear Associative Memory

To resolve the limitations of coarse granularity and routing ambiguity inherent in dense rank-r updates, we depart from the conventional view of LoRA as monolithic blocks, instead reconceptualizing both the weight matrix and its updates as a *Linear Associative Memory*.

Definition 3.1 (Weight Matrix as Linear Associative Memory)**.** Consider a weight matrix $\mathbf{W} \in \mathbb{R}^{d_{\text{out}} \times d_{\text{in}}}$ of rank m. Through the lens of linear associative memory (Kohonen, 1972; Anderson, 1972), a weight matrix $\mathbf{W} \in \mathbb{R}^{d_{\text{out}} \times d_{\text{in}}}$ of rank m acts as a retrieval system composed of m atomic key-value pairs $\{(\mathbf{k}_i, \mathbf{v}_i)\}_{i=1}^{m}$, where $\mathbf{k}_i \in \mathbb{R}^{d_{\text{in}}}$ and $\mathbf{v}_i \in \mathbb{R}^{d_{\text{out}}}$ such that $\mathbf{W} \approx \sum_{i=1}^{m} \mathbf{v}_i \mathbf{k}_i^\top$. For an input hidden state for a token $\mathbf{x} \in \mathbb{R}^{d_{\text{in}}}$, the matrix-vector product effectively

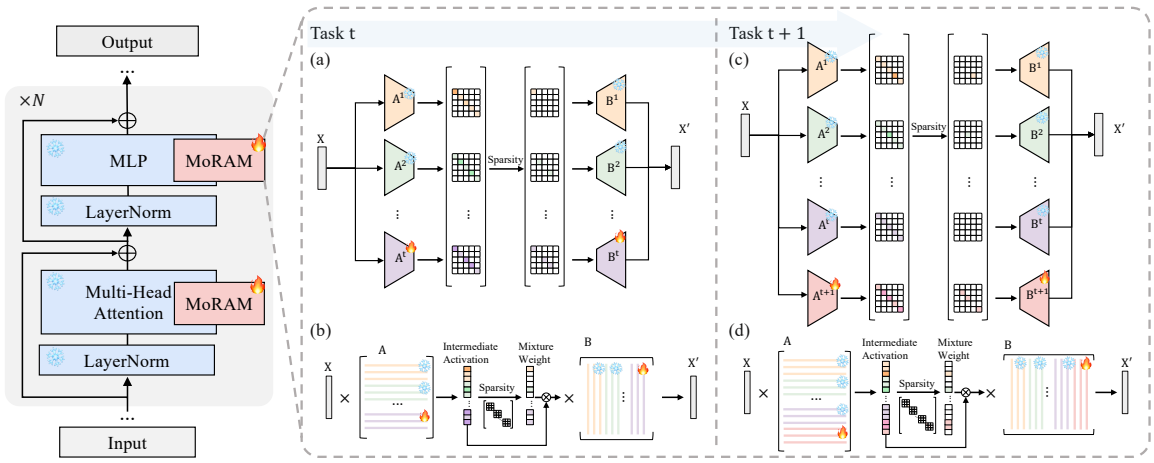

Figure 2. Overview of MoRAM. For each new task, we freeze the ranks learned on previous tasks and introduce r new ranks of updates. Our sparse self-activated mixture-of-ranks framework jointly considers all old and new ranks, adaptively inferring a sparse mixture weight for each rank. Panels (a,c) illustrate MoRAM conceptually and (b,d) detail its computation for tasks t and $t+1$, respectively.

performs a content-addressable read operation:

$$\mathbf{y} = \mathbf{W}\mathbf{x} \approx \sum_{i=1}^{m} \mathbf{v}_i(\mathbf{k}_i^\top \mathbf{x}), \tag{2}$$

where the inner product $(\mathbf{k}_i^\top \mathbf{x})$ computes the *relevance* (or activation strength) of the i-th memory slot to the input, which weights the retrieval of the value vector $\mathbf{v}_i$.

Remark 3.2 (Key-Value Memory of Weight Matrix). It is crucial to distinguish Definition 3.1 from the key-value mechanism in Self-Attention (Vaswani et al., 2017). In attention, keys and values are *dynamic* projections of the input sequence generated at runtime. In contrast, under the linear associative memory view, the keys $\mathbf{k}_i$ and values $\mathbf{v}_i$ are *static* parameters intrinsic to the weight matrix, representing knowledge patterns acquired during pre-training.

3.3. Proposed MoRAM

3.3.1. Mixture of Rank-1 Memory Experts

Fine-grained rank-1 memory augmentation. Grounded by the associative memory view (Definition 3.1), we reconceptualize the fine-tuning process. Instead of formulating the update $\Delta\mathbf{W}$ as a single-unit rank-r matrix, we treat it as a collection of retrievable rank-1 memory augmentations. Formally, we define the update as the aggregation of r atomic rank-1 key-value pair updates:

$$\Delta\mathbf{W}\mathbf{x} = \sum_{i=1}^{r} \underbrace{\mathbf{B}_{:,i}}_{\text{Value } \mathbf{v}_i} \big(\underbrace{\mathbf{A}_{i,:}}_{\text{Key } \mathbf{k}_i^\top} \mathbf{x} \big), \tag{3}$$

where the row vector $\mathbf{A}_{i,:}$ acts as the **Key** determining the relevance of the atom to the input, and the column vector $\mathbf{B}_{:,i}$ acts as the **Value** storing the retrieved knowledge. Crucially, this shifts the paradigm from matrix adaptation to *memory expansion*: the update is no longer a rigid block, but a flexible set of fine-grained atomic memories.

Despite this granular potential, standard LoRA and its variants (Hu et al., 2021; Meng et al., 2024; Zhang et al., 2024a) apply updates densely: every rank contributes to every input. Even in MoE-LoRA, while experts are separated at rank-r adapter level, the constituent rank-1 memories *within* each expert remain entangled: (1) *Interference*: Irrelevant knowledge subspaces within a chosen expert are forced to activate for mismatched inputs. (2) *Routing collapse*: It overlooks the intrinsic capacity of the key vectors $\mathbf{A}$ to act as *content retrieval keys*, instead relying on indiscriminate dense activation or redundant external routers.

MoRAM formulation. To address this, we propose **MoRAM** (**M**ixture **o**f **R**ank-1 **A**ssociative **M**emory). We dismantle the rigid adapter structure, redefining the model's adaptation parameters as a dynamic collection of atomic memory experts $\mathcal{M}_t = \{(\mathbf{B}_{:,i}, \mathbf{A}_{i,:})\}_{i=1}^{r_t}$, where r_t denotes the total accumulated rank-1 pairs avaliable at task t. For an input $\mathbf{x}$ during task t (with accumulated memory atoms r_t), the effective update is defined as a sparse, input-dependent mixture:

$$\Delta\mathbf{W}^t = \sum_{i=1}^{r_t} \mathrm{w}_i \mathbf{B}_{:,i}\mathbf{A}_{i,:}, \tag{4}$$

where $\mathrm{w}_i \in \mathbb{R}$ represents the computed retrieval confidence of the i-th memory atom on each input token hidden state $\mathbf{x}$. This formulation allows the model to freeze specific "atomic" memories (preserving old tasks) while inserting new ones on demand of input, or to jointly activate a combination of old and new memory slots to handle shared concepts.

3.3.2. Self-Activation for MoRAM Routing

Relying on the key-value form of the rank-1 adapter, we propose a self-activation mechanism for routing the memory

experts. We derive the mixing weights directly from the intrinsic activation of each atomic memory, leveraging the key vectors $\mathbf{A}_{i,:}$ for memory retrieval. Unlike standard MoE approaches that rely on additional routing networks, our self-activation routing performs routing as a content-addressable retrieval, reducing the possibility of forgetting caused by an additional router.

Self-activated relevance scoring. By eliminating the external router, MoRAM avoids the optimization instability and forgetting associated with auxiliary networks. Instead, we derive mixing weights directly from the intrinsic alignment between the input and the memory keys. Formally, for an input token $\mathbf{x} \in \mathbb{R}^{d_{\text{in}}}$ and the set of accumulated memory atoms up to task t, we compute the raw relevance score s_i for the i-th atom as:

$$\mathrm{s}_i \;=\; \frac{\mathbf{A}_{i,:}\mathbf{x}}{\sqrt{\sum_{j=1}^{r_t}(\mathbf{A}_{j,:}\mathbf{x})^2}}, \tag{5}$$

where the numerator represents the relevance to the memory key $\mathbf{A}_{i,:}$, the denominator performs an ℓ_2-normalization across the entire memory ensemble for numerical stability. Empirically, we find that this intrinsic scoring mechanism matches or exceeds the performance of external routers (see Table 4), confirming that the memory keys alone contain sufficient information to determine their own utility.

3.3.3. Sparse Expert Routing and Mixture

While Eq. (5) measures relevance, naive dense activation leads to low specialty and induces interference and computational overhead. We therefore employ sparse routing to enhance fine-grained specialization of the fine-grained experts and routers.

Sparse rank selection. To prevent interference between tasks and ensure a budgeted computational cost, we enforce a sparsity constraint via `top-k` masking. Given the raw relevance scores s, we retain only the k entries with the highest activation and mask the rest:

$$[\mathrm{TopK}(\mathrm{s}, k)]_i = \begin{cases} \mathrm{s}_i, & \text{if } \mathrm{s}_i \in \text{top-}k(\mathrm{s}), \\ -\infty, & \text{otherwise.} \end{cases} \tag{6}$$

This masking ensures that for any given input, at most k out of the total r_t accumulated memory atoms are eligible for activation. This encourages rank specialization: only a small set of the most relevant ranks are emphasized and trained to capture each kind of input-specific dynamics, and it prevents tiny, noisy activations from spuriously triggering unrelated memory atoms (*e.g.*, those frozen from prior tasks).

Sharpness enhancement. To further encourage rank specialization and concentrate the update on the most relevant ranks, we apply temperature-scaled softmax normalization to enhance the sharpness of the mixture weights:

$$\mathrm{w}_i \;=\; \mathrm{softmax}\Big(\frac{\mathrm{TopK}(\mathrm{s}, k)}{\tau_{\text{MoRAM}}}\Big)_i, \tag{7}$$

where τ_{MoRAM} is a scalar temperature hyperparameter. In the forward pass, a lower τ_{MoRAM} acts as a contrast enhancer, concentrating probability mass on the definitive specialist ranks. In the backward pass, it functions as a gradient router: by sharpening the distribution, stronger learning signals are directed exclusively to the winning ranks. This effectively isolates them from irrelevant updates and accelerates specialization, ensuring that memory atoms only evolve when they are truly relevant to the current data distribution.

Threshold-based expert selection. To maximize retrieval precision during inference, we apply an additional threshold-based expert selection, via a relevance threshold δ to the normalized scores, enabling adaptively pruning memory atoms with weak activation signals. Since the number of useful experts may differ depending on layers and input, at inference time, we apply this threshold-based filter to further adaptively select experts from the top-k experts, while reducing both computational overhead and noise:

$$\mathrm{w}_i := \mathbb{1}\{\mathrm{s}_i \geq \delta\} \odot \mathrm{w}_i. \tag{8}$$

This operation yields a highly sparse, input-dependent set comprising only the most significant memory experts.

3.3.4. Continual Learning with MoRAM

Incremental memory expansion. Unlike methods that add fixed-size adapter blocks (Yu et al., 2024), MoRAM expands memory "little by little." For each new task, we introduce a set of r new atomic rank-1 pairs (Keys $\mathbf{A}$ and Values $\mathbf{B}$), freeze all prior atoms, and let the self-activation mechanism jointly route across the union of all old and new memories. This seamlessly integrates new knowledge while preserving the reusability of prior tasks. To enhance efficiency and enable sub-linear expansion rate, MoRAM supports low-utility atoms to be pruned after training with minimal performance degradation (more in Appendix A.10).

Training objectives. In our experiments, we only use the model's standard training objective, without any extra regularization or load-balancing constraints. Benefiting from the fine-grained modeling with rank-1 experts, the experts tend to be special and the routing tend to be balance and stable naturally. Even without additional regularization, the specialized experts and router causes router degeradation and forgetting not seriously, while we beleive furher regularization might be more helpful. In practice, we empirically observe that conventional load-balancing regularization (Shazeer et al., 2017; Lepikhin et al., 2020; Fedus et al., 2022; Dai et al., 2024) for MoE may not be necessary for the experimented setup. And imposing regularization

Table 1. Comparisons on X-TAIL for each domain in terms of "Transfer", "Average", and "Last" scores (%). The **best** and the **second best** results are highlighted in **red** and **blue**, respectively.

Method	Aircraft	Caltech	DTD	EuroSAT	Flowers	Food	MNIST	OxPet	Cars	SUN397	*Average*
CLIP											
Zero-shot	23.5	76.8	37.3	36.7	63.6	84.0	46.7	86.7	66.1	63.7	58.5
Fine-tune	39.6	84.7	70.0	94.7	97.0	85.8	97.6	93.4	81.0	74.7	81.9
Transfer											
Zero-shot (Radford et al., 2021)	–	**76.8**	**37.3**	36.7	63.6	84.0	**46.7**	86.7	**66.1**	**63.7**	62.4
LwF (Li & Hoiem, 2017)	–	66.6	26.9	19.5	51.0	78.4	26.6	68.9	35.5	56.1	47.7
WiSE-FT (Wortsman et al., 2022)	–	70.1	31.9	25.3	56.3	79.8	29.9	74.9	45.6	56.8	52.3
iCaRL (Rebuffi et al., 2017)	–	71.7	35.0	43.0	63.4	**86.9**	43.9	87.8	63.7	60.0	61.7
ZSCL (Zheng et al., 2023)	–	73.3	32.6	36.8	62.1	83.8	42.1	83.6	56.5	60.2	59.0
MoE-Adapter (Yu et al., 2024)	–	71.0	34.9	19.2	63.0	**86.6**	20.0	87.2	63.7	58.6	56.0
RAIL-Primal (Xu et al., 2024)	–	**76.8**	**37.3**	36.7	63.6	84.0	**46.7**	86.7	**66.1**	**63.7**	62.4
CoDyRA (Lu et al., 2024)	–	74.3	36.8	**44.2**	**69.9**	83.5	42.8	**88.9**	64.6	**63.4**	**63.2**
MoRAM	–	**74.5**	**38.1**	**46.9**	**65.3**	82.9	**45.8**	**88.2**	**65.1**	62.9	**63.3**
Average											
LwF (Li & Hoiem, 2017)	24.7	79.7	38.3	36.9	63.9	81.0	36.5	71.9	42.7	56.7	53.2
WiSE-FT (Wortsman et al., 2022)	27.1	76.5	40.9	31.3	68.7	81.6	31.4	74.7	51.7	58.4	54.2
iCaRL (Rebuffi et al., 2017)	25.4	72.1	37.5	51.6	65.1	**87.1**	59.1	88.0	63.7	60.1	61.0
ZSCL (Zheng et al., 2023)	36.0	75.0	40.7	40.5	71.0	85.3	46.3	83.3	60.7	61.5	60.0
MoE-Adapter (Yu et al., 2024)	**43.6**	77.9	52.1	34.7	75.9	**86.3**	45.2	87.4	66.6	60.2	63.0
RAIL-Primal (Xu et al., 2024)	42.4	**89.8**	55.7	68.5	**84.0**	83.3	**65.3**	85.8	**67.9**	**64.5**	70.7
CoDyRA (Lu et al., 2024)	41.4	81.0	**58.7**	**77.8**	83.4	84.6	64.5	**90.4**	67.2	**64.4**	**71.3**
MoRAM	**44.1**	**81.6**	**64.6**	**79.6**	**83.9**	84.4	**66.5**	**89.7**	**68.4**	64.1	**72.7**
Last											
LwF (Li & Hoiem, 2017)	25.5	72.1	38.9	55.4	65.5	**87.3**	81.9	88.6	63.6	61.5	64.0
WiSE-FT (Wortsman et al., 2022)	21.8	76.8	42.9	20.8	77.5	84.9	30.7	76.6	75.8	72.5	58.0
iCaRL (Rebuffi et al., 2017)	25.5	72.1	38.9	55.4	65.5	**87.3**	81.9	88.6	63.6	61.5	64.0
ZSCL (Zheng et al., 2023)	33.1	75.3	43.5	35.2	74.6	**87.4**	50.4	84.2	77.3	73.4	63.4
MoE-Adapter (Yu et al., 2024)	**43.2**	78.7	57.6	32.8	79.4	86.0	86.7	87.8	**78.2**	**74.2**	70.5
RAIL-Primal (Xu et al., 2024)	**41.7**	**94.0**	**66.0**	86.4	**97.2**	82.4	93.1	83.6	75.0	71.3	79.1
CoDyRA (Lu et al., 2024)	37.7	**81.5**	65.1	**89.9**	91.4	85.5	**96.8**	**93.3**	77.3	73.5	**79.2**
MoRAM	37.7	**81.5**	**70.7**	**92.4**	**95.0**	86.0	**97.6**	**92.6**	**81.0**	**74.7**	**80.9**

on the self-activation routing improperly tends to hinder the learning of the key vectors, since the key vectors for routing are also crucial for information representation.

4. Experiments

In this paper, we conduct experiments across a diverse set of tasks, including continual learning for both vision-language CLIP models and LMs, and analyze catastrophic forgetting during fine-tuning. Detailed implementation settings and more experiment results are provided in Appendix A.1.

4.1. Experimental Results

Continual Learning of CLIP. We evaluate X-TAIL performance in Table 1, reporting *Transfer*, *Last*, and *Average* accuracy (MTIL results in Appendix Table 12). While prior methods (Yu et al., 2024; Xu et al., 2024) are constrained by the base model's zero-shot ceiling, MoRAM follows (Zheng et al., 2023; Lu et al., 2024) to continuously adapt, surpassing this limit and achieving superior Last and Average scores. Critically, MoRAM enhances representation without the external domain-IDs or feature banks required by (Yu et al., 2024; Xu et al., 2024), and improves upon the fixed weighting in (Lu et al., 2024) by utilizing dynamic, input-dependent gating for finer expert specialization.

Continual Learning of LLMs. In Table 2, we evaluate MoRAM on LLaMA (Dubey et al., 2024) and Gemma (Team et al., 2024) using the TRACE benchmark (Wang et al., 2023b). Traditional regularization (Kirkpatrick et al., 2017), rehearsal (Lopez-Paz & Ranzato, 2017), and prompt-based (Wang et al., 2022f) methods struggle to scale, often underperforming simple In-Context Learning. Among LoRA variants, naive SeqLoRA suffers significant forgetting, while recent approaches like O-LoRA (Wang et al., 2023a), HiDeLoRA (Wang et al., 2025), and TreeLoRA (Qian et al., 2025) rely on rigid orthogonality or complex structural expansions. In contrast, MoRAM performs robustly on LLMs, achieving results competitive with existing methods. We provide additional evaluations on language classification tasks in Tables 8 and 9 of Appendix.

Forgetting and generalization after standard fine-tuning. Table 3 examines how standard fine-tuning affects both in-domain performance and out-of-domain generalization. *(1) Forgetting:* Dense LoRA updates overwrite pre-trained knowledge, degrading performance on semantically distant topics (*e.g.*, Religions). *(2) Positive transfer:* Conversely, code adaptation improves logically related tasks

Table 2. Comparison with a broad range of CL methods on the TRACE benchmark. We report Overall Performance (OP (%) ↑) and Backward Transfer (BWT (%) ↓). Results are averaged over three runs with standard deviations. The best results are highlighted in bold.

	FIX(ICL)	SeqLoRA	OGD	GEM	EWC	L2P	DualPrompt	HiDeLoRA	O-LoRA	TreeLoRA	MoRAM
meta-llama / LLaMA-2-7B-Chat											
OP	38.94 ± 0.3	34.3 ± 1.2	42.09 ± 1.6	40.08 ± 1.6	42.36 ± 1.2	36.23 ± 0.8	37.69 ± 1.2	41.60 ± 0.8	42.78 ± 0.8	43.52 ± 1.0	**44.54 ± 0.9**
BWT	–	18.5 ± 0.8	8.06 ± 1.2	6.77 ± 1.2	5.97 ± 0.8	8.25 ± 0.8	8.03 ± 0.8	7.12 ± 0.4	7.16 ± 0.4	3.46 ± 0.4	**1.37 ± 0.3**
google / Gemma-2B-it											
OP	32.3 ± 0.2	31.89 ± 0.8	32.85 ± 1.4	26.48 ± 1.5	28.35 ± 1.6	31.14 ± 1.2	32.42 ± 1.0	33.25 ± 0.9	33.73 ± 0.8	33.41 ± 0.9	**36.27 ± 0.7**
BWT	–	15.28 ± 0.4	12.27 ± 0.9	18.25 ± 0.9	16.96 ± 1.2	15.77 ± 0.7	14.25 ± 0.5	13.66 ± 0.5	12.36 ± 0.4	8.50 ± 0.5	**2.74 ± 0.4**
meta-llama / LLaMA-3-1B-Instruct											
OP	31.16 ± 0.4	29.73 ± 1.6	30.12 ± 2.0	32.19 ± 2.0	31.96 ± 1.6	29.38 ± 1.2	30.76 ± 1.2	33.73 ± 1.2	32.94 ± 0.8	36.14 ± 0.7	**37.77 ± 0.8**
BWT	–	17.03 ± 1.2	15.2 ± 1.6	10.74 ± 1.6	11.62 ± 1.2	13.57 ± 0.8	11.34 ± 0.8	12.36 ± 0.8	12.89 ± 1.2	7.36 ± 0.8	**3.12 ± 0.8**

Table 3. Standard fine-tuning of Llama-3.1-8B on CodeAlpaca. We report zero-shot in-domain performance on HumanEval (Pass@1) for the code generation and out-of-domain accuracy on selected MMLU subjects (formal logic, philosophy, world religions, economics, public relations, STEM, physics, machine learning). The last two columns report trainable parameters (for MoRAM: added / activated).

Method	HumanEval (Pass@1)	Out-of-Domain (Acc.)									Params (M)	%Params
		Logic	Phil.	Reli.	Econ.	Pub. Rel.	STEM	Phys.	ML	MMLU		
Llama-3.1-8B	38.40	42.06	**71.06**	**83.63**	70.17	**68.18**	54.84	39.22	**40.18**	63.45	—	—
LoRA ($r = 4$)	41.46	39.68	70.09	81.87	71.43	65.45	54.77	**45.10**	40.17	63.28	10.5	0.13%
LoRA ($r = 8$)	44.51	39.68	**70.74**	81.87	71.85	64.54	54.17	42.16	39.29	63.03	21.0	0.26%
LoRA ($r = 16$)	**45.73**	41.27	68.49	80.70	**72.69**	**66.36**	54.96	44.11	38.39	63.35	41.9	0.52%
LoRA ($r = 32$)	**47.56**	**42.85**	69.45	81.87	72.27	**66.36**	**55.44**	**45.10**	39.29	**63.59**	83.9	1.03%
MoRAM	**47.56**	**48.41**	70.09	**82.46**	**73.53**	**68.18**	**55.53**	**46.08**	**41.96**	**63.70**	41.9/**26.2**	0.52%/**0.32%**

(*e.g.*, STEM, Logic), indicating valid transfer potential.

In contrast, MoRAM leverages its atomic memory structure, treating updates as independent rank-1 memory atoms rather than entangled blocks, the model isolates new knowledge accumulation from existing representations. This granular independence prevents the catastrophic overwriting of unrelated concepts (*e.g.*, Religions) while the content-addressable self-activation ensures that relevant atoms are reused for logical tasks (*e.g.*, STEM, Logic). Consequently, MoRAM achieves superior out-of-domain accuracy using roughly one-third of the active parameters required by a standard rank-32 LoRA.

4.2. Visualizations of Rank-1 Memory Activations

Figure 3 shows rank activations recorded during continual learning. These visualizations illustrate two properties of MoRAM: (1) individual ranks specialize on distinct input patterns, and (2) the model substantially reduces cross-task interference, thereby mitigating forgetting. Extended visualizations across more tasks and scenarios appear in Fig. 6 and Fig. 7 in the Appendix.

Each rank specializes in distinct input patterns. In Fig. 3a, airplane patches strongly activate Rank 0, while blue-sky backgrounds predominantly activate Rank 11. In Fig. 3c, Ranks 19, 20, and 29 (orange boxes) respond to jaguar patches. The more complex backgrounds in Fig. 3c (*e.g.*, leaves, shadows) yield a richer, more distributed pattern than the simple blue sky in Fig. 3a, highlighting MoRAM 's capacity to model contextual complexity. Some ranks learned earlier are also reused on later tasks (Fig. 7, Appendix), indicating transfer of shared semantics.

Reduced interference and mitigated forgetting. Comparing the same input after Task 1 (Fig. 3a) and after Task 2 (Fig. 3b) shows almost identical activations (more in Fig. 6, Appendix): Rank 0 still responds to airplane semantics and Rank 11 to blue-sky patches. This stability indicates that our self-activated, sparse mixture-of-ranks prevents later updates from overwriting earlier task representations, reducing interference and mitigating forgetting.

4.3. Ablation Studies

Ablation of memory retrieval strategies. Table 4 analyzes the impact of different retrieval mechanisms under a controlled setup. (1) *MoE-LoRA (Coarse Baseline)* employs a router to weight entire adapters. Its coarse granularity forces the simultaneous activation of conflicting subspaces, leading to significant interference and forgetting. (2) *External Router* applies a separately learned router to individual rank-1 atoms. However, decoupling the routing logic from the memory content leads to *retrieval collapse*: as the number of atoms grows, the external router struggles to index them precisely, resulting in worse performance than the coarse baseline. (3) *Self-Activated Retrieval* replaces the external router with intrinsic key-value matching (Eq. 5). By ensuring the retrieval condition is strictly aligned with the expert's content, it resolves the routing ambiguity without extra parameters. (4) *Sparsity Constraint (Top-k)* enforces a strict activation budget. This serves as a gating mechanism that prevents memory collisions and reduces interference

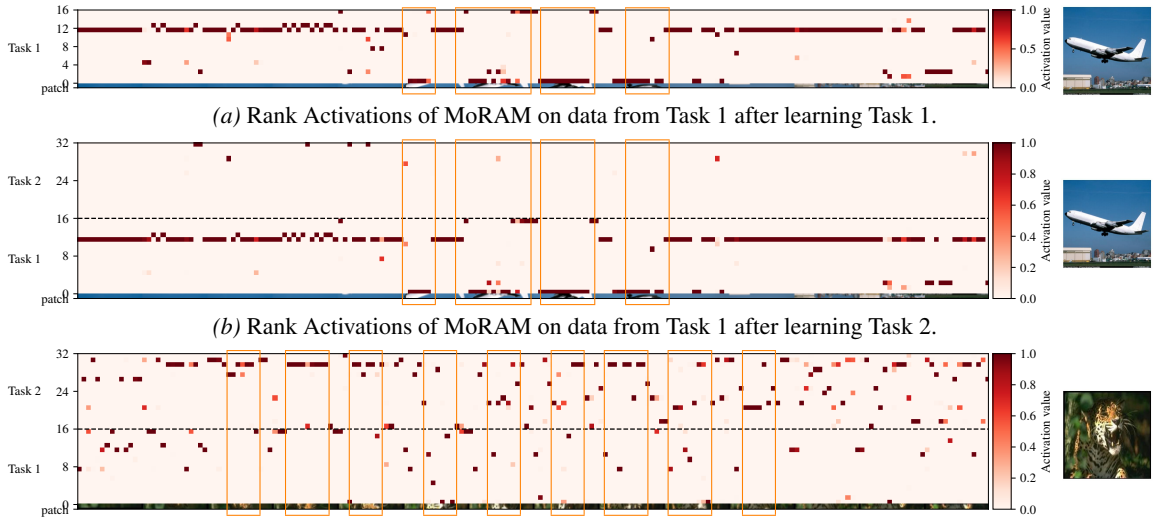

(a) Rank Activations of MoRAM on data from Task 1 after learning Task 1.

(b) Rank Activations of MoRAM on data from Task 1 after learning Task 2.

(c) Rank Activations of MoRAM on data from Task 2 after learning Task 2.

Figure 3. Visualization of MoRAM rank activations during Task 1 and Task 2 training. Activations are extracted from the K projection in the attention module (layer 8) of the image encoder. Corresponding image patches are shown below each activation map, with regions relevant to each class marked by orange bounding boxes. Zoom in for details. More visualizations are in Figs. 6 and 7 of the Appendix, demonstrating forgetting mitigation and knowledge reuse.

Table 4. Routing Strategies

Routing	Transfer	Average	Last
MoE-LoRA (Coarse Baseline)	62.56	69.45	74.53
External Router (Learned W_r)	60.09	65.97	69.76
Self-Activated Retrieval	60.26	65.94	69.85
w/ Sparsity Constraint (Top-k)	60.69	66.52	70.62
w/ Temperature Scaling (τ_{MoRAM})	62.07	71.15	79.62
w/ Threshold-based expert selection (δ)	60.78	66.83	71.08
MoRAM (Full)	**63.30**	**72.70**	**80.90**

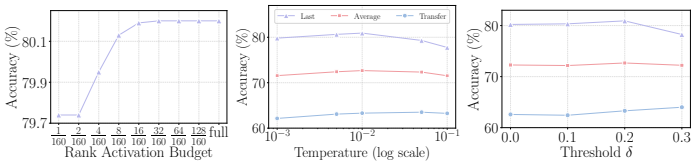

(a) Acti. Budget *(b)* Temp. τ_{MoRAM} *(c)* Thre. δ

Figure 4. Ablation on (a) rank activation budget, (b) temperature τ_{MoRAM}, and (c) threshold δ.

during training. (5) *Temperature Scaling* sharpens the retrieval distribution. This concentrates gradient flow on the most relevant "specialist" atoms, accelerating their adaptation while protecting shared memories. (6) *Threshold-based selection* prunes weak activation signals (δ) strictly at test time, maximizing retrieval precision by eliminating noise.

Rank Activation Budget. We probe rank usage by varying the activation budget on a 10-task checkpoint (Fig. 4a). To isolate this effect, we disable other sparsity mechanisms (*e.g.*, thresholding). Performance improves as the budget increases from 2 to 16 (10% of total ranks) before plateauing, confirming that a small, sparse subset of specialized ranks suffices to cover diverse inputs. Crucially, accuracy remains robust even at high budgets, demonstrating that self-activation naturally prioritizes relevant signals while suppressing noise, even without strict sparsity constraints.

Sharpness enhancement. Temperature scaling (Eq. (7)) modulates activation sparsity: lower τ_{MoRAM} concentrates probability mass, while higher τ_{MoRAM} broadens expert participation. Fig. 4b demonstrates that higher τ_{MoRAM} significantly boosts transfer to unseen tasks (even surpassing SOTA in Table 1). However, we select a moderate τ_{MoRAM} of 0.01 to optimally balance specificity (retention) and generalization (transfer), ensuring strong overall performance.

Threshold-based rank selection. Figure 4c shows the effect of the test-time rank selection threshold δ. Applying a modest threshold removes low-activation ranks and reduces noisy contributions, which improves both downstream adaptation and out-of-domain generalization.

5. Conclusion

We presented MoRAM, a framework that challenges the coarse-grained design of standard MoE-LoRA. By redefining adaptation as the accumulation of atomic associative memories, we demonstrated that high-performing CL does not require complex external routers, but rather precise, content-addressable retrieval of low-rank atomic memories.
Future works. MoRAM controls mixture sharpness and sparsity via top-k selection, temperature scaling, and thresholding. While effective, the sparse activation mechanism can be further improved by incorporating awareness of the input data distribution. Learning this temperature or adapting the mixture's sharpness based on data offers a promising avenue for future research. We also aim to extend the method's applicability to a broader range of PTMs and applications.

Impact Statement

MoRAM's sparse mixture-of-ranks method makes continual adaptation of large vision–language and language models far more efficient and reliable. By updating only the most relevant low-rank subspaces, it reduce compute and memory requirements, enabling on-device personalization in domains like education, healthcare, and finance. This democratizes access to powerful, continually evolved models for smaller teams and resource-constrained settings, driving innovation and improving quality of life. Preserving pre-trained knowledge also ensures stability in safety-critical systems, such as medical diagnostics and autonomous vehicles, where forgetting of pre-trained capabilities can be dangerous.

The focus of this paper is fundamental research, and is broadly applicable to model fine-tuning techniques. Thus, it is possible that MoRAM 's lightweight updates could be misused to insert stealthy backdoors or reinforce hidden biases that are hard to detect. Because it leaves most pre-trained parameters untouched, existing biases may persist or become entrenched. To mitigate these risks, we recommend strict audit logging of rank-level updates, anomaly detection on sparse changes, robust access controls, and routine bias and fairness assessments alongside any deployment.

References

Aghajanyan, A., Zettlemoyer, L., and Gupta, S. Intrinsic dimensionality explains the effectiveness of language model fine-tuning. *arXiv preprint arXiv:2012.13255*, 2020.

Aljundi, R., Babiloni, F., Elhoseiny, M., Rohrbach, M., and Tuytelaars, T. Memory aware synapses: Learning what (not) to forget. In *Proceedings of the European conference on computer vision (ECCV)*, pp. 139–154, 2018.

Aljundi, R., Kelchtermans, K., and Tuytelaars, T. Task-free continual learning. In *Proceedings of the IEEE/CVF Conference on Computer Vision and Pattern Recognition*, pp. 11254–11263, 2019a.

Aljundi, R., Lin, M., Goujaud, B., and Bengio, Y. Gradient based sample selection for online continual learning. *Advances in neural information processing systems*, 32, 2019b.

Anderson, J. A. A simple neural network generating an interactive memory. *Mathematical biosciences*, 14(3-4): 197–220, 1972.

Biderman, D., Portes, J., Ortiz, J. J. G., Paul, M., Greengard, P., Jennings, C., King, D., Havens, S., Chiley, V., Frankle, J., et al. Lora learns less and forgets less. *arXiv preprint arXiv:2405.09673*, 2024.

Bossard, L., Guillaumin, M., and Van Gool, L. Food-101–mining discriminative components with random forests. In *Proceedings of the European conference on computer vision (ECCV)*, pp. 446–461, 2014.

Chaudhary, S. Code alpaca: An instruction-following llama model for code generation. https://github.com/sahil280114/codealpaca, 2023.

Chaudhry, A., Dokania, P. K., Ajanthan, T., and Torr, P. H. Riemannian walk for incremental learning: Understanding forgetting and intransigence. In *Proceedings of the European conference on computer vision (ECCV)*, pp. 532–547, 2018a.

Chaudhry, A., Ranzato, M., Rohrbach, M., and Elhoseiny, M. Efficient lifelong learning with a-gem. *arXiv preprint arXiv:1812.00420*, 2018b.

Chen, M., Tworek, J., Jun, H., Yuan, Q., Pinto, H. P. D. O., Kaplan, J., Edwards, H., Burda, Y., Joseph, N., Brockman, G., et al. Evaluating large language models trained on code. *arXiv preprint arXiv:2107.03374*, 2021.

Chen, S., Jie, Z., and Ma, L. Llava-mole: Sparse mixture of lora experts for mitigating data conflicts in instruction finetuning mllms. *arXiv preprint arXiv:2401.16160*, 2024.

Chen, Z., Wang, Z., Wang, Z., Liu, H., Yin, Z., Liu, S., Sheng, L., Ouyang, W., Qiao, Y., and Shao, J. Octavius: Mitigating task interference in mllms via lora-moe. *arXiv preprint arXiv:2311.02684*, 2023.

Cimpoi, M., Maji, S., Kokkinos, I., Mohamed, S., and Vedaldi, A. Describing textures in the wild. In *Proceedings of the IEEE conference on computer vision and pattern recognition*, pp. 3606–3613, 2014.

Dai, D., Deng, C., Zhao, C., Xu, R., Gao, H., Chen, D., Li, J., Zeng, W., Yu, X., Wu, Y., et al. Deepseekmoe: Towards ultimate expert specialization in mixture-of-experts language models. *arXiv preprint arXiv:2401.06066*, 2024.

De Lange, M., Aljundi, R., Masana, M., Parisot, S., Jia, X., Leonardis, A., Slabaugh, G., and Tuytelaars, T. A continual learning survey: Defying forgetting in classification tasks. *IEEE transactions on pattern analysis and machine intelligence*, 44(7):3366–3385, 2021.

de Masson D'Autume, C., Ruder, S., Kong, L., and Yogatama, D. Episodic memory in lifelong language learning. *Advances in Neural Information Processing Systems*, 32, 2019.

Deng, L. The mnist database of handwritten digit images for machine learning research [best of the web]. *IEEE signal processing magazine*, 29(6):141–142, 2012.

Ding, N., Lv, X., Wang, Q., Chen, Y., Zhou, B., Liu, Z., and Sun, M. Sparse low-rank adaptation of pre-trained language models. *arXiv preprint arXiv:2311.11696*, 2023.

Ding, Y., Liu, L., Tian, C., Yang, J., and Ding, H. Don't stop learning: Towards continual learning for the clip model. *arXiv preprint arXiv:2207.09248*, 2022.

Dosovitskiy, A., Beyer, L., Kolesnikov, A., Weissenborn, D., Zhai, X., Unterthiner, T., Dehghani, M., Minderer, M., Heigold, G., Gelly, S., et al. An image is worth 16x16 words: Transformers for image recognition at scale. *arXiv preprint arXiv:2010.11929*, 2020.

Dou, S., Zhou, E., Liu, Y., Gao, S., Zhao, J., Shen, W., Zhou, Y., Xi, Z., Wang, X., Fan, X., et al. Loramoe: Alleviate world knowledge forgetting in large language models via moe-style plugin. *arXiv preprint arXiv:2312.09979*, 2023.

Dubey, A., Jauhri, A., Pandey, A., Kadian, A., Al-Dahle, A., Letman, A., Mathur, A., Schelten, A., Yang, A., Fan, A., et al. The llama 3 herd of models. *arXiv e-prints*, pp. arXiv–2407, 2024.

Fedus, W., Zoph, B., and Shazeer, N. Switch transformers: Scaling to trillion parameter models with simple and efficient sparsity. *Journal of Machine Learning Research*, 23(120):1–39, 2022.

Fei-Fei, L., Fergus, R., and Perona, P. Learning generative visual models from few training examples: An incremental bayesian approach tested on 101 object categories. In *2004 conference on computer vision and pattern recognition workshop*, pp. 178–178. IEEE, 2004.

Gao, L., Tow, J., Abbasi, B., Biderman, S., Black, S., DiPofi, A., Foster, C., Golding, L., Hsu, J., Le Noac'h, A., Li, H., McDonell, K., Muennighoff, N., Ociepa, C., Phang, J., Reynolds, L., Schoelkopf, H., Skowron, A., Sutawika, L., Tang, E., Thite, A., Wang, B., Wang, K., and Zou, A. The language model evaluation harness, 07 2024. URL https://zenodo.org/records/12608602.

Garg, S., Farajtabar, M., Pouransari, H., Vemulapalli, R., Mehta, S., Tuzel, O., Shankar, V., and Faghri, F. Ticclip: Continual training of clip models. *arXiv preprint arXiv:2310.16226*, 2023.

Grattafiori, A., Dubey, A., Jauhri, A., Pandey, A., Kadian, A., Al-Dahle, A., Letman, A., Mathur, A., Schelten, A., Vaughan, A., et al. The llama 3 herd of models. *arXiv e-prints*, pp. arXiv–2407, 2024.

Hadsell, R., Rao, D., Rusu, A. A., and Pascanu, R. Embracing change: Continual learning in deep neural networks. *Trends in cognitive sciences*, 24(12):1028–1040, 2020.

He, X. O. Mixture of a million experts. *arXiv preprint arXiv:2407.04153*, 2024.

Helber, P., Bischke, B., Dengel, A., and Borth, D. Eurosat: A novel dataset and deep learning benchmark for land use and land cover classification. *IEEE Journal of Selected Topics in Applied Earth Observations and Remote Sensing*, 12(7):2217–2226, 2019.

Hendrycks, D., Burns, C., Basart, S., Zou, A., Mazeika, M., Song, D., and Steinhardt, J. Measuring massive multitask language understanding. *Proceedings of the International Conference on Learning Representations (ICLR)*, 2021.

Hu, E. J., Shen, Y., Wallis, P., Allen-Zhu, Z., Li, Y., Wang, S., Wang, L., and Chen, W. Lora: Low-rank adaptation of large language models. *arXiv preprint arXiv:2106.09685*, 2021.

Jha, S., Gong, D., Zhao, H., and Yao, L. Npcl: Neural processes for uncertainty-aware continual learning. *arXiv preprint arXiv:2310.19272*, 2023.

Jha, S., Gong, D., and Yao, L. CLAP4CLIP: Continual learning with probabilistic finetuning for vision-language models. In *The Thirty-eighth Annual Conference on Neural Information Processing Systems*, 2024. URL https://openreview.net/forum?id=rF1YRtZfoJ.

Kirkpatrick, J., Pascanu, R., Rabinowitz, N., Veness, J., Desjardins, G., Rusu, A. A., Milan, K., Quan, J., Ramalho, T., Grabska-Barwinska, A., et al. Overcoming catastrophic forgetting in neural networks. *Proceedings of the national academy of sciences*, 114(13):3521–3526, 2017.

Kohonen, T. Correlation matrix memories. *IEEE transactions on computers*, 100(4):353–359, 1972.

Krause, J., Stark, M., Deng, J., and Fei-Fei, L. 3d object representations for fine-grained categorization. In *Proceedings of the IEEE international conference on computer vision workshops*, pp. 554–561, 2013.

Krizhevsky, A., Hinton, G., et al. Learning multiple layers of features from tiny images. 2009.

Lepikhin, D., Lee, H., Xu, Y., Chen, D., Firat, O., Huang, Y., Krikun, M., Shazeer, N., and Chen, Z. Gshard: Scaling giant models with conditional computation and automatic sharding. *arXiv preprint arXiv:2006.16668*, 2020.

Li, C., Farkhoor, H., Liu, R., and Yosinski, J. Measuring the intrinsic dimension of objective landscapes. *arXiv preprint arXiv:1804.08838*, 2018.

Li, D., Ma, Y., Wang, N., Ye, Z., Cheng, Z., Tang, Y., Zhang, Y., Duan, L., Zuo, J., Yang, C., et al. Mixlora: Enhancing large language models fine-tuning with lora-based

mixture of experts. *arXiv preprint arXiv:2404.15159*, 2024.

Li, H., Lin, S., Duan, L., Liang, Y., and Shroff, N. Theory on mixture-of-experts in continual learning. In *The Thirteenth International Conference on Learning Representations*, 2025. URL https://openreview.net/forum?id=7XgKAabsPp.

Li, Z. and Hoiem, D. Learning without forgetting. *IEEE transactions on pattern analysis and machine intelligence*, 40(12):2935–2947, 2017.

Liang, Y.-S. and Li, W.-J. Inflora: Interference-free low-rank adaptation for continual learning. In *Proceedings of the IEEE/CVF Conference on Computer Vision and Pattern Recognition*, pp. 23638–23647, 2024.

Liu, Y., Su, Y., Liu, A.-A., Schiele, B., and Sun, Q. Mnemonics training: Multi-class incremental learning without forgetting. In *Proceedings of the IEEE/CVF conference on Computer Vision and Pattern Recognition*, pp. 12245–12254, 2020.

Liu, Z., Lyn, J., Zhu, W., Tian, X., and Graham, Y. Alora: Allocating low-rank adaptation for fine-tuning large language models. *arXiv preprint arXiv:2403.16187*, 2024.

Lopez-Paz, D. and Ranzato, M. Gradient episodic memory for continual learning. *Advances in neural information processing systems*, 30, 2017.

Loshchilov, I. and Hutter, F. Decoupled weight decay regularization. *arXiv preprint arXiv:1711.05101*, 2017.

Lu, H., Zhao, C., Xue, J., Yao, L., Moore, K., and Gong, D. Adaptive rank, reduced forgetting: Knowledge retention in continual learning vision-language models with dynamic rank-selective lora. *arXiv preprint arXiv:2412.01004*, 2024.

Ludziejewski, J., Krajewski, J., Adamczewski, K., Pióro, M., Krutul, M., Antoniak, S., Ciebiera, K., Król, K., Odrzygóźdź, T., Sankowski, P., Cygan, M., and Jaszczur, S. Scaling laws for fine-grained mixture of experts. In *Forty-first International Conference on Machine Learning*, 2024. URL https://openreview.net/forum?id=yoqdlynCRs.

Luo, Z., Liu, Y., Schiele, B., and Sun, Q. Class-incremental exemplar compression for class-incremental learning. In *Proceedings of the IEEE/CVF Conference on Computer Vision and Pattern Recognition*, pp. 11371–11380, 2023.

Maji, S., Rahtu, E., Kannala, J., Blaschko, M., and Vedaldi, A. Fine-grained visual classification of aircraft. *arXiv preprint arXiv:1306.5151*, 2013.

McCloskey, M. and Cohen, N. J. Catastrophic interference in connectionist networks: The sequential learning problem. In *Psychology of learning and motivation*, volume 24, pp. 109–165. Elsevier, 1989.

McDonnell, M. D., Gong, D., Parvaneh, A., Abbasnejad, E., and van den Hengel, A. Ranpac: Random projections and pre-trained models for continual learning. *Advances in Neural Information Processing Systems*, 36, 2024.

Meng, F., Wang, Z., and Zhang, M. Pissa: Principal singular values and singular vectors adaptation of large language models. *arXiv preprint arXiv:2404.02948*, 2024.

Nguyen, C. V., Achille, A., Lam, M., Hassner, T., Mahadevan, V., and Soatto, S. Toward understanding catastrophic forgetting in continual learning. *arXiv preprint arXiv:1908.01091*, 2019.

Nilsback, M.-E. and Zisserman, A. Automated flower classification over a large number of classes. In *2008 Sixth Indian conference on computer vision, graphics & image processing*, pp. 722–729. IEEE, 2008.

Parkhi, O. M., Vedaldi, A., Zisserman, A., and Jawahar, C. Cats and dogs. In *2012 IEEE conference on computer vision and pattern recognition*, pp. 3498–3505. IEEE, 2012.

Qian, Y.-Y., Xu, Y.-Z., Zhang, Z.-Y., Zhao, P., and Zhou, Z.-H. Treelora: Efficient continual learning via layer-wise loras guided by a hierarchical gradient-similarity tree. *arXiv preprint arXiv:2506.10355*, 2025.

Qiao, F. and Mahdavi, M. Learn more, but bother less: parameter efficient continual learning. *Advances in Neural Information Processing Systems*, 37:97476–97498, 2024.

Qin, C. and Joty, S. Lfpt5: A unified framework for lifelong few-shot language learning based on prompt tuning of t5. *arXiv preprint arXiv:2110.07298*, 2021.

Radford, A., Kim, J. W., Hallacy, C., Ramesh, A., Goh, G., Agarwal, S., Sastry, G., Askell, A., Mishkin, P., Clark, J., et al. Learning transferable visual models from natural language supervision. In *International conference on machine learning*, pp. 8748–8763. PMLR, 2021.

Raffel, C., Shazeer, N., Roberts, A., Lee, K., Narang, S., Matena, M., Zhou, Y., Li, W., and Liu, P. J. Exploring the limits of transfer learning with a unified text-to-text transformer. *Journal of machine learning research*, 21 (140):1–67, 2020.

Razdaibiedina, A., Mao, Y., Hou, R., Khabsa, M., Lewis, M., and Almahairi, A. Progressive prompts: Continual learning for language models. *arXiv preprint arXiv:2301.12314*, 2023.

Rebuffi, S.-A., Kolesnikov, A., Sperl, G., and Lampert, C. H. icarl: Incremental classifier and representation learning. In *Proceedings of the IEEE conference on Computer Vision and Pattern Recognition*, pp. 2001–2010, 2017.

Rusu, A. A., Rabinowitz, N. C., Desjardins, G., Soyer, H., Kirkpatrick, J., Kavukcuoglu, K., Pascanu, R., and Hadsell, R. Progressive neural networks. *arXiv preprint arXiv:1606.04671*, 2016.

Shazeer, N., Mirhoseini, A., Maziarz, K., Davis, A., Le, Q., Hinton, G., and Dean, J. Outrageously large neural networks: The sparsely-gated mixture-of-experts layer. *arXiv preprint arXiv:1701.06538*, 2017.

Smith, J. S., Karlinsky, L., Gutta, V., Cascante-Bonilla, P., Kim, D., Arbelle, A., Panda, R., Feris, R., and Kira, Z. Coda-prompt: Continual decomposed attention-based prompting for rehearsal-free continual learning. In *Proceedings of the IEEE/CVF Conference on Computer Vision and Pattern Recognition*, pp. 11909–11919, 2023.

Tang, L., Tian, Z., Li, K., He, C., Zhou, H., Zhao, H., Li, X., and Jia, J. Mind the interference: Retaining pre-trained knowledge in parameter efficient continual learning of vision-language models. In *European Conference on Computer Vision*, pp. 346–365. Springer, 2025.

Team, G., Mesnard, T., Hardin, C., Dadashi, R., Bhupatiraju, S., Pathak, S., Sifre, L., Rivière, M., Kale, M. S., Love, J., et al. Gemma: Open models based on gemini research and technology. *arXiv preprint arXiv:2403.08295*, 2024.

Touvron, H., Martin, L., Stone, K., Albert, P., Almahairi, A., Babaei, Y., Bashlykov, N., Batra, S., Bhargava, P., Bhosale, S., et al. Llama 2: Open foundation and fine-tuned chat models. *arXiv preprint arXiv:2307.09288*, 2023.

Vaswani, A., Shazeer, N., Parmar, N., Uszkoreit, J., Jones, L., Gomez, A. N., Kaiser, Ł., and Polosukhin, I. Attention is all you need. *Advances in neural information processing systems*, 30, 2017.

Wang, A., Singh, A., Michael, J., Hill, F., Levy, O., and Bowman, S. R. Glue: A multi-task benchmark and analysis platform for natural language understanding. *arXiv preprint arXiv:1804.07461*, 2018.

Wang, A., Pruksachatkun, Y., Nangia, N., Singh, A., Michael, J., Hill, F., Levy, O., and Bowman, S. Superglue: A stickier benchmark for general-purpose language understanding systems. *Advances in neural information processing systems*, 32, 2019.

Wang, F.-Y., Zhou, D.-W., Liu, L., Ye, H.-J., Bian, Y., Zhan, D.-C., and Zhao, P. Beef: Bi-compatible class-incremental learning via energy-based expansion and fusion. In *The Eleventh International Conference on Learning Representations*, 2022a.

Wang, F.-Y., Zhou, D.-W., Ye, H.-J., and Zhan, D.-C. Foster: Feature boosting and compression for class-incremental learning. In *European conference on computer vision*, pp. 398–414. Springer, 2022b.

Wang, H., Lu, H., Yao, L., and Gong, D. Self-expansion of pre-trained models with mixture of adapters for continual learning. *arXiv preprint arXiv:2403.18886*, 2024.

Wang, L., Xie, J., Zhang, X., Su, H., and Zhu, J. Hide-pet: continual learning via hierarchical decomposition of parameter-efficient tuning. *IEEE Transactions on Pattern Analysis and Machine Intelligence*, 2025.

Wang, X., Chen, T., Ge, Q., Xia, H., Bao, R., Zheng, R., Zhang, Q., Gui, T., and Huang, X. Orthogonal subspace learning for language model continual learning. *arXiv preprint arXiv:2310.14152*, 2023a.

Wang, X., Zhang, Y., Chen, T., Gao, S., Jin, S., Yang, X., Xi, Z., Zheng, R., Zou, Y., Gui, T., et al. Trace: A comprehensive benchmark for continual learning in large language models. *arXiv preprint arXiv:2310.06762*, 2023b.

Wang, Y., Huang, Z., and Hong, X. S-prompts learning with pre-trained transformers: An occam's razor for domain incremental learning. *Advances in Neural Information Processing Systems*, 35:5682–5695, 2022c.

Wang, Y., Mishra, S., Alipoormolabashi, P., Kordi, Y., Mirzaei, A., Arunkumar, A., Ashok, A., Dhanasekaran, A. S., Naik, A., Stap, D., et al. Super-naturalinstructions: Generalization via declarative instructions on 1600+ nlp tasks. *arXiv preprint arXiv:2204.07705*, 2022d.

Wang, Z., Zhang, Z., Ebrahimi, S., Sun, R., Zhang, H., Lee, C.-Y., Ren, X., Su, G., Perot, V., Dy, J., et al. Dualprompt: Complementary prompting for rehearsal-free continual learning. In *European Conference on Computer Vision*, pp. 631–648. Springer, 2022e.

Wang, Z., Zhang, Z., Lee, C.-Y., Zhang, H., Sun, R., Ren, X., Su, G., Perot, V., Dy, J., and Pfister, T. Learning to prompt for continual learning. In *Proceedings of the IEEE/CVF Conference on Computer Vision and Pattern Recognition*, pp. 139–149, 2022f.

Wortsman, M., Ilharco, G., Kim, J. W., Li, M., Kornblith, S., Roelofs, R., Lopes, R. G., Hajishirzi, H., Farhadi, A., Namkoong, H., et al. Robust fine-tuning of zero-shot models. In *Proceedings of the IEEE/CVF Conference on Computer Vision and Pattern Recognition*, pp. 7959–7971, 2022.

Wu, T., Wang, J., Zhao, Z., and Wong, N. Mixture-of-subspaces in low-rank adaptation. *arXiv preprint arXiv:2406.11909*, 2024a.

Wu, X., Huang, S., and Wei, F. Mixture of loRA experts. In *The Twelfth International Conference on Learning Representations*, 2024b. URL https://openreview.net/forum?id=uWvKBCYh4S.

Wu, Y., Piao, H., Huang, L.-K., Wang, R., Li, W., Pfister, H., Meng, D., Ma, K., and Wei, Y. Sd-lora: Scalable decoupled low-rank adaptation for class incremental learning. *arXiv preprint arXiv:2501.13198*, 2025.

Xiao, J., Hays, J., Ehinger, K. A., Oliva, A., and Torralba, A. Sun database: Large-scale scene recognition from abbey to zoo. In *2010 IEEE computer society conference on computer vision and pattern recognition*, pp. 3485–3492. IEEE, 2010.

Xu, Y., Chen, Y., Nie, J., Wang, Y., Zhuang, H., and Okumura, M. Advancing cross-domain discriminability in continual learning of vision-language models. *Advances in Neural Information Processing Systems*, 37:51552–51576, 2024.

Yan, Q., Gong, D., Liu, Y., van den Hengel, A., and Shi, J. Q. Learning bayesian sparse networks with full experience replay for continual learning. In *Proceedings of the IEEE/CVF Conference on Computer Vision and Pattern Recognition*, pp. 109–118, 2022.

Yan, S., Xie, J., and He, X. Der: Dynamically expandable representation for class incremental learning. In *Proceedings of the IEEE/CVF Conference on Computer Vision and Pattern Recognition*, pp. 3014–3023, 2021.

Yang, S., Ali, M. A., Wang, C.-L., Hu, L., and Wang, D. Moral: Moe augmented lora for llms' lifelong learning. *arXiv preprint arXiv:2402.11260*, 2024.

Yoon, J., Kim, S., Yang, E., and Hwang, S. J. Scalable and order-robust continual learning with additive parameter decomposition. In *International Conference on Learning Representations*, 2020. URL https://openreview.net/forum?id=r1gdj2EKPB.

Yu, J., Zhuge, Y., Zhang, L., Hu, P., Wang, D., Lu, H., and He, Y. Boosting continual learning of vision-language models via mixture-of-experts adapters. In *Proceedings of the IEEE/CVF Conference on Computer Vision and Pattern Recognition*, pp. 23219–23230, 2024.

Zenke, F., Poole, B., and Ganguli, S. Continual learning through synaptic intelligence. In *International conference on machine learning*, pp. 3987–3995. PMLR, 2017.

Zhang, J., Zhao, Y., Chen, D., Tian, X., Zheng, H., and Zhu, W. Milora: Efficient mixture of low-rank adaptation for large language models fine-tuning. *arXiv preprint arXiv:2410.18035*, 2024a.

Zhang, J., You, J., Panda, A., and Goldstein, T. Lori: Reducing cross-task interference in multi-task low-rank adaptation. *arXiv preprint arXiv:2504.07448*, 2025.

Zhang, Q., Chen, M., Bukharin, A., Karampatziakis, N., He, P., Cheng, Y., Chen, W., and Zhao, T. Adalora: Adaptive budget allocation for parameter-efficient fine-tuning. *arXiv preprint arXiv:2303.10512*, 2023.

Zhang, W., Janson, P., Aljundi, R., and Elhoseiny, M. Overcoming generic knowledge loss with selective parameter update. In *Proceedings of the IEEE/CVF Conference on Computer Vision and Pattern Recognition*, pp. 24046–24056, 2024b.

Zhang, X., Zhao, J., and LeCun, Y. Character-level convolutional networks for text classification. *Advances in neural information processing systems*, 28, 2015.

Zhao, W., Wang, S., Hu, Y., Zhao, Y., Qin, B., Zhang, X., Yang, Q., Xu, D., and Che, W. Sapt: A shared attention framework for parameter-efficient continual learning of large language models. *arXiv preprint arXiv:2401.08295*, 2024.

Zheng, Y., Zhang, R., Zhang, J., Ye, Y., Luo, Z., Feng, Z., and Ma, Y. Llamafactory: Unified efficient fine-tuning of 100+ language models. In *Proceedings of the 62nd Annual Meeting of the Association for Computational Linguistics (Volume 3: System Demonstrations)*, Bangkok, Thailand, 2024. Association for Computational Linguistics. URL http://arxiv.org/abs/2403.13372.

Zheng, Z., Ma, M., Wang, K., Qin, Z., Yue, X., and You, Y. Preventing zero-shot transfer degradation in continual learning of vision-language models. *arXiv preprint arXiv:2303.06628*, 2023.

Zhou, D.-W., Wang, Q.-W., Ye, H.-J., and Zhan, D.-C. A model or 603 exemplars: Towards memory-efficient class-incremental learning. *arXiv preprint arXiv:2205.13218*, 2022.

Zhou, D.-W., Sun, H.-L., Ye, H.-J., and Zhan, D.-C. Expandable subspace ensemble for pre-trained model-based class-incremental learning. In *Proceedings of the IEEE/CVF Conference on Computer Vision and Pattern Recognition*, pp. 23554–23564, 2024.

A. Additional Details and Results of Experiments

A.1. Detailed Experiment Settings

Continual Learning of CLIP on X-TAIL and MTIL. The MTIL setting consists of 1,201 classes drawn from 11 diverse datasets: Aircraft (Maji et al., 2013), Caltech101 (Fei-Fei et al., 2004), CIFAR100 (Krizhevsky et al., 2009), DTD (Cimpoi et al., 2014), EuroSAT (Helber et al., 2019), Flowers (Nilsback & Zisserman, 2008), Food (Bossard et al., 2014), MNIST (Deng, 2012), OxfordPet (Parkhi et al., 2012), Cars (Krause et al., 2013), and SUN397 (Xiao et al., 2010). In the X-TAIL setting, a total of 10 datasets are used, with CIFAR100 (Fei-Fei et al., 2004) excluded to prevent domain overlap, following the protocol in (Xu et al., 2024). In line with (Xu et al., 2024), we use a 5-shot split for MTIL and a 16-shot split for X-TAIL.

We follow the experimental setups in (Zheng et al., 2023; Yu et al., 2024; Xu et al., 2024) and use the CLIP model with a ViT-B/16 backbone (Radford et al., 2021) for all experiments. By default, MoRAM is applied to every pre-trained weight matrix in both the vision and text encoders, with an initial rank of 16 per update. Each task is trained for 500 iterations using AdamW (Loshchilov & Hutter, 2017) with a learning rate of $5e-4$. During continual learning, we freeze the ranks learned from previous tasks and initialize new $r = 16$ ranks for each incoming task. The rank activation budget is set to 16 throughout all tasks. We set the temperature $\tau_{\text{MoRAM}} = 0.1$ and the threshold $\delta = 0.2$.

Continual Learning of LLMs on TRACE. We evaluate MoRAM on the TRACE benchmark (Wang et al., 2023b), a comprehensive suite designed to assess continual learning in LLMs such as LLaMA (Touvron et al., 2023) and Gemma (Team et al., 2024). TRACE standardizes eight diverse datasets spanning domain-specific understanding (C-STANCE, FOMC), reasoning (ScienceQA, NumGLUE-cm/ds), summarization (MeetingBank), code generation (Py150), and multilingual simplification (20Minuten). Following standard protocols, each task consists of 5,000 training and 2,000 testing examples. We employ task-specific metrics to capture performance nuances: Accuracy for classification and reasoning tasks; ROUGE-L for summarization; SARI for simplification; and similarity scores for code generation.

We adopt the variable epoch schedule from Qian et al. (2025) ($\{2, 1, 3, 2, 1, 2, 2, 3\}$ epochs). For each incoming task, we initialize $r = 16$ new ranks while maintaining a fixed rank activation budget of $k = 16$ across all tasks. We set the softmax temperature $\tau_{\text{MoRAM}} = 0.03$ and the inference threshold $\delta = 0.2$. Optimization proceeds with a learning rate of 1×10^{-4} and a batch size of 4, utilizing a maximum context length of 1024 tokens. All experiments leverage DeepSpeed ZeRO-2 with BF16 mixed-precision on a cluster of four Nvidia H100 GPUs.

Continual Learning of LMs on language classification tasks. We follow the protocol of previous work in continually fine-tuning the T5-large (Raffel et al., 2020) and LLaMA2-7B (Touvron et al., 2023) on a suite of text-classification tasks. We train on five standard benchmarks—AG News, Amazon Reviews, Yelp Reviews, DBpedia, and Yahoo Answers—using three distinct task orderings drawn from (Qin & Joty, 2021; Razdaibiedina et al., 2023; Wang et al., 2023a; Qiao & Mahdavi, 2024). To probe longer sequences, we extend this to a 15-dataset stream (Table 5), incorporating tasks from the original CL benchmark (Zhang et al., 2015), GLUE (Wang et al., 2018), SuperGLUE (Wang et al., 2019), and the IMDB movie reviews corpus. Natural language prompts for each task are presented in Table 6, with NLI tasks (MNLI, RTE, CB), sentiment classification (Amazon, Yelp, SST-2, IMDB), and topic classification (AG News, DBpedia, Yahoo).

We evaluate three distinct task sequences for both the standard CL and 15-task benchmarks (Table 7). After completing the final task in each stream, we report the average accuracy across all tasks. All experiments use one epoch per task with DeepSpeed, a fixed learning rate of $1e-3$, batch size 64, and dropout of 0.1. MoRAM is applied to both the query and key projection matrices within attention layers, initializing $r = 8$ new ranks for each incoming task similarly as in (Wang et al., 2023a; Qiao & Mahdavi, 2024). We maintain a constant activation budget of 4 ranks throughout continual learning, set the temperature $\tau_{\text{MoRAM}} = 0.1$, and the threshold $\delta = 0.2$.

Generalization and forgetting on unseen tasks after standard fine-tuning. To assess effects on pre-trained general knowledge, we fine-tune Llama3.1-8B (Grattafiori et al., 2024) on the CodeAlpaca code-generation dataset (Chaudhary, 2023) using llama-Factory (Zheng et al., 2024) and evaluate using lm-eval-harness (Gao et al., 2024) on zero-shot in-domain performance on HumanEval (Chen et al., 2021), as well as out-of-domain accuracy on a broad selection of MMLU (Hendrycks et al., 2021) subjects—Formal Logic, Philosophy, World Religions, Economics, Public Relations, STEM, Physics, and Machine Learning.

In this experiment, MoRAM is applied to all linear weight matrices of the pre-trained model. We fine-tune on CodeAlpaca with a batch size of 32 over 3 epochs and a cosine learning-rate schedule starting at $5e-4$. We train with $r = 16$ ranks and enforce a constant activation budget of 4 ranks. The self-routed gating uses a temperature $\tau_{\text{MoRAM}} = 0.5$ and a threshold $\delta = 0.2$. We observe that, due to variations in hidden representations across architectures, the optimal temperature setting can differ across each pre-trained models.

Table 5. Details of the 15 datasets used in our continual-learning experiments using LMs. NLI denotes natural language inference, and QA denotes question-answering tasks. The first five tasks comprise the standard CL benchmark; the remaining ten tasks are used for the extended long-sequence evaluations.

Dataset name	Category	Task	Domain	Metric
1. Yelp	CL Benchmark	sentiment analysis	Yelp reviews	accuracy
2. Amazon	CL Benchmark	sentiment analysis	Amazon reviews	accuracy
3. DBpedia	CL Benchmark	topic classification	Wikipedia	accuracy
4. Yahoo	CL Benchmark	topic classification	Yahoo Q&A	accuracy
5. AG News	CL Benchmark	topic classification	news	accuracy
6. MNLI	GLUE	NLI	various	accuracy
7. QQP	GLUE	paragraph detection	Quora	accuracy
8. RTE	GLUE	NLI	news, Wikipedia	accuracy
9. SST-2	GLUE	sentiment analysis	movie reviews	accuracy
10. WiC	SuperGLUE	word sense disambiguation	lexical databases	accuracy
11. CB	SuperGLUE	NLI	various	accuracy
12. COPA	SuperGLUE	QA	blogs, encyclopedia	accuracy
13. BoolQA	SuperGLUE	boolean QA	Wikipedia	accuracy
14. MultiRC	SuperGLUE	QA	various	accuracy
15. IMDB	SuperGLUE	sentiment analysis	movie reviews	accuracy

Table 6. Instructions for different tasks.

Task	Prompts
NLI	What is the logical relationship between the "sentence 1" and the "sentence 2"? Choose one from the option.
QQP	Whether the "first sentence" and the "second sentence" have the same meaning? Choose one from the option.
SC	What is the sentiment of the following paragraph? Choose one from the option.
TC	What is the topic of the following paragraph? Choose one from the option.
BoolQA	According to the following passage, is the question true or false? Choose one from the option.
MultiRC	According to the following passage and question, is the candidate answer true or false? Choose one from the option.
WiC	Given a word and two sentences, whether the word is used with the same sense in both sentence? Choose one from the option.

A.2. Evaluation Metrics

To strictly evaluate the plasticity and stability of our method, we employ the following metrics. Let N denote the total number of learned tasks, and $A_{i,j}$ denote the performance (e.g., accuracy, ROUGE, or similarity score) on task j after training on task i.

CLIP Continual Learning Metrics. For the CLIP experiments (MTIL and X-TAIL), we report the following metrics as in (Zheng et al., 2023; Yu et al., 2024; Xu et al., 2024):

- **Transfer Accuracy (Transfer):** indicates the model's zero-shot performance on future domains before they are learned, measures the extent to which the pre-trained zero-shot ability is preserved (or improved) throughout incremental learning.
- **Average Accuracy (Average):** indicates the average accuracy of all learning steps across all domains. It captures the comprehensive performance stability throughout the entire incremental training process.
- **Last Accuracy (Last):** represent the model's performance on all seen domains after the training is fully completed.

LLM Continual Learning Metrics. For the TRACE benchmark, we adopt the standard metrics as in (Wang et al., 2023b):

- **Overall Performance (OP):** The average performance across all learned tasks at the end of training.

$$\text{OP} = \frac{1}{N}\sum_{j=1}^{N} A_{N,j}, \tag{9}$$

Table 7. The six task-sequence orders used in our continual learning experiments. Sequences 1–3 follow the standard CL benchmarks employed in prior work. Sequences 4–6 extend to longer 15-task streams, as introduced in (Razdaibiedina et al., 2023).

Order	Task Sequence
1	dbpedia → amazon → yahoo → ag
2	dbpedia → amazon → ag → yahoo
3	yahoo → amazon → ag → dbpedia
4	mnli → cb → wic → copa → qqp → boolqa → rte → imdb → yelp → amazon → sst-2 → dbpedia → ag → multirc → yahoo
5	multirc → boolqa → wic → mnli → cb → copa → qqp → rte → imdb → sst-2 → dbpedia → ag → yelp → amazon → yahoo
6	yelp → amazon → mnli → cb → copa → qqp → rte → imdb → sst-2 → dbpedia → ag → yahoo → multirc → boolqa → wic

Table 8. Summary of results on standard CL benchmarks with T5-large. We report averaged accuracy after training on the last task across three task orderings.

	Standard CL Benchmark			
Method	Order-1	Order-2	Order-3	*Avg.*
MTL		80.0		
SeqFT	18.9	24.9	41.7	28.5
SeqLoRA	44.6	32.7	53.7	43.7
IncLoRA	66.0	64.9	68.3	66.4
Replay	55.2	56.9	61.3	57.8
EWC	48.7	47.7	54.5	50.3
LwF	54.4	53.1	49.6	52.3
L2P	60.3	61.7	61.1	60.7
LFPT5	67.6	72.6	77.9	72.7
InfLoRA	75.2	75.4	75.8	75.5
O-LoRA	75.4	75.7	76.3	75.8
LB-CL	76.9	76.5	76.8	76.7
MoRAM	**77.4**	**77.5**	**77.9**	**77.6**

where $A_{i,j}$ represents the performance on task j after learning task i.

- **Backward Transfer (BWT):** Measures the average performance degradation (forgetting) of previous tasks $j < N$ after learning new tasks. A lower BWT indicates less forgetting (better stability).

$$\text{BWT} = \frac{1}{N-1} \sum_{j=1}^{N-1} (A_{j,j} - A_{N,j}) \qquad (10)$$

A.3. Continual Learning of LMs on the Standard-CL benchmark.

Table 8 reports results across three task orderings: MoRAM consistently outperforms prior methods and closely approaches the multi-task learning (MTL) upper bound. Unlike O-LoRA (Wang et al., 2023a) and LB-CL (Qiao & Mahdavi, 2024), which rely on orthogonality constraints or gradient projections between per-task LoRA adapters (potentially limiting adapter capacity), MoRAM needs no extra regularization. By decomposing each rank-r update into rank-one components and applying self-activated, sparse gating, MoRAM lets each component specialize on its own input distribution, reducing interference and more effectively capturing diverse patterns. We further evaluate MoRAM on LLaMA2-7B (Touvron et al., 2023) under the same continual-learning setup (Table 10 in the Appendix), MoRAM also outperforms O-LoRA by 2.3% averaged over 3 task orders.

Table 9. Average accuracy on T5-large continual-learning benchmarks after the final task, evaluated over extended 15-task sequences. Results for prior methods are taken from (Qiao & Mahdavi, 2024).

	Large Number of Tasks			
Method	Order-4	Order-5	Order-6	*Avg.*
MTL		76.5		
SeqFT	7.4	7.4	7.5	7.4
SeqLoRA	2.3	0.6	1.9	1.6
IncLoRA	63.3	58.5	61.7	61.2
Replay	55	54.6	53.1	54.2
EWC	45.3	44.5	45.6	45.1
LwF	50.1	43.1	47.4	46.9
L2P	57.5	53.8	56.9	56.1
LFPT5	69.8	67.2	69.2	68.7
O-LoRA	**70.5**	65.5	70.5	68.8
LB-CL	68.4	67.3	71.8	69.2
MoRAM	68.91	**68.32**	**71.95**	**69.72**

Table 10. Continual learning results on standard CL benchmarks with the LLaMA2-7B model.

Method	Order-1	Order-2	Order-3	*Avg.*
O-LoRA	76.8	75.7	75.7	76.1
MoRAM	**77.8**	**78.0**	**79.3**	**78.4**

A.4. Continual Learning of LMs on Long Task Sequences

In Table 8, we evaluate MoRAM on standard CL benchmarks (Razdaibiedina et al., 2023). In Table 9, we extend the evaluation to challenged long task sequences using 15 datasets with 3 different orderings as in (Wang et al., 2023a; Qiao & Mahdavi, 2024). Consistent with the findings in

Table 8, MoRAM outperforms previous methods in terms of averaged performance across three task orders, and largely close the gap to multi-task learning. Two key design choices drive this robust performance in the long-sequence regime. First, by decomposing each LoRA update into fine-grained rank-1 components and enforcing a small, fixed activation budget, MoRAM encourages each rank to specialize on a narrow subspace of the data manifold. At inference time, only the most relevant subspaces are activated for a given input, which preserves earlier task representations and prevents catastrophic interference. Second, our self-routed gating mechanism enables each rank to assess its own relevance on a per-token basis, yielding stable mixture patterns as the expert pool grows. Coupling with our proposed rank pruning, these mechanisms ensure that MoRAM continually incorporates new knowledge only when needed while robustly maintaining prior capabilities.

Table 11. Comparisons of trainable parameters for each pre-trained weight matrix during continual learning of each task. MoE-LoRA and MoE-Adapter trains additional router module with LoRA experts. In MoRAM, k denotes the rank activation budget (with $k \leq r$).

Method	Trainable parameters per task
LoRA (Hu et al., 2021)	$r\,(d_{\text{in}} + d_{\text{out}})$
MoE-LoRA (1 expert/task)	$r\,(d_{\text{in}} + d_{\text{out}}) \;+\; d_{\text{in}}$
MoE-Adapter (2 experts/task) (Yu et al., 2024)	$2(r\,(d_{\text{in}} + d_{\text{out}}) + d_{\text{in}})$
CoDyRA (Lu et al., 2024)	$r\,(d_{\text{in}} + d_{\text{out}}) + r$
O-LoRA (Wang et al., 2023a)	$r\,(d_{\text{in}} + d_{\text{out}})$
LB-CL (Qiao & Mahdavi, 2024)	$r\,(d_{\text{in}} + d_{\text{out}}) + r$
MoRAM	$rd_{\text{in}} + kd_{\text{out}}$

A.5. Multi-domain task incremental learning.

We evaluate MoRAM in the few-shot MTIL setting (Table 12) under the same protocols as (Yu et al., 2024; Xu et al., 2024; Lu et al., 2024). Consistent with the results observed in the X-TAIL setting, our method demonstrates clear superiority in this scenario.

In this challenging scenario, the model must learn 11 diverse tasks sequentially, with only five examples per class. These findings validate that our self-activated sparse mixture-of-ranks framework both facilitates continual acquisition of new knowledge and mitigates forgetting from the pre-trained model and earlier tasks.

A.6. More Comparisons on CL on LMs

Results on SuperNI benchmark. To provide a complete comparison, we additionally evaluate MoRAM against SAPT (Zhao et al., 2024) on the SuperNI benchmark (Wang et al., 2022d) using the T5-Large backbone (Table 13). We report results in both replay-based and replay-free settings. Under the replay-based protocol introduced by SAPT, where pseudo-samples are generated using a trained generative model, MoRAM attains a stronger stability–plasticity trade-off (AP: 51.79% vs. 51.54%; FT: 0.73% vs. 0.91%). In the replay-free setting, which is the primary use case for MoRAM, our method achieves state-of-the-art performance (AP: 39.62%) and substantially outperforms parameter-efficient baselines such as O-LoRA (26.37%) and L2P (15.18%). These results highlight the complementary design choices. SAPT improves replay efficiency through shared attention prompts, while MoRAM relies on architectural isolation via sparse rank-1 experts. As a result, MoRAM remains effective without a memory buffer, yet can also incorporate replay to further improve performance beyond SAPT.

Discussions on performance robustness. To assess order robustness, we incorporate the OPD metric proposed by (Yoon et al., 2020), which measures a model's sensitivity to the sequence of arriving tasks. Following standard practice for evaluating global performance stability, we compute the standard deviation of the final average accuracy over the K task orders considered. In Table 14, using results on the Standard CL Benchmark with three distinct task orders, MoRAM demonstrates substantially improved robustness to task ordering. The disparity across orders is 0.26 for MoRAM, which is approximately half of that of O-LoRA (0.46). This indicates that the Self-Activated Sparse Mixture mechanism effectively reduces task interference and mitigates the unidirectional knowledge transfer effects identified in prior work.

A.7. More Comparison on HumanEval for Code Generation

To further evaluate code generation performance, we compare MoRAM against LoRI-D and LoRI-S (Zhang et al., 2025) on the HumanEval benchmark (Table 15). MoRAM consistently outperforms both LoRI variants across all metrics, achieving notable improvements in Pass@1, Pass@5, and especially Pass@10.

A.8. Robustness

MoRAM employs a sparse mixture of previously learned and newly introduced rank-1 experts to capture both shared and task-specific knowledge, resulting in substantially improved Last performance. To assess statistical significance and robustness, we report mean and standard deviation over three independent runs (Table 16). MoRAM consistently outperforms competing methods across all metrics and exhibits lower variance, highlighting its effectiveness and stability in continual-learning scenarios.

A.9. More comparisons on X-TAIL

To further validate MoRAM 's robustness, we evaluated it under other continual-learning task orderings, i.e., X-TAIL

Table 12. Comparisons on 5-shot MTIL setting. Following the same protocol as in (Yu et al., 2024; Xu et al., 2024; Lu et al., 2024).

Method	Aircraft	Caltech101	CIFAR100	DTD	EuroSAT	Flowers	Food	MNIST	OxfordPet	Cars	SUN397	*Average*
CLIP												
Zero-shot (Radford et al., 2021)	24.3	88.4	68.2	44.6	54.9	71.0	88.5	59.4	89.0	64.7	65.2	65.3
Transfer												
Zero-shot (Radford et al., 2021)	–	88.4	68.2	44.6	**54.9**	**71.0**	**88.5**	59.6	89.0	**64.7**	**65.2**	69.4
LwF (Li & Hoiem, 2017)	–	72.1	49.2	35.9	44.5	41.1	66.6	50.5	69.0	19.0	51.7	50.0
LwF-VR (Ding et al., 2022)	–	82.2	62.5	40.1	40.1	56.3	80.0	60.9	77.6	40.5	60.8	60.1
WiSE-FT (Wortsman et al., 2022)	–	77.6	60.0	41.3	39.4	53.0	76.6	58.1	75.5	37.3	58.2	57.7
ZSCL (Zheng et al., 2023)	–	84.0	68.1	44.8	46.8	63.6	84.9	61.4	81.4	55.5	62.2	65.3
MoE-Adapter (Yu et al., 2024)	–	87.9	68.2	44.1	48.1	64.7	**88.8**	**69.0**	**89.1**	64.5	**65.1**	68.9
RAIL-Primal (Xu et al., 2024)	–	88.4	68.2	44.6	**54.9**	**71.0**	**88.5**	59.6	89.0	**64.7**	**65.2**	69.4
CoDyRA (Lu et al., 2024)	–	**92.4**	**68.4**	**45.8**	**54.5**	**69.6**	87.4	**65.2**	88.5	64.2	64.5	**69.9**
MoRAM	–	**92.0**	**68.8**	**45.6**	53.1	68.6	84.4	64.3	**89.8**	**65.4**	64.8	**69.7**
Average												
LwF (Li & Hoiem, 2017)	23.5	77.4	43.5	41.7	43.5	52.2	54.6	63.4	68.0	21.3	52.6	49.2
LwF-VR (Ding et al., 2022)	24.9	89.1	64.2	53.4	54.3	70.8	79.2	66.5	79.2	44.1	61.6	62.5
WiSE-FT (Wortsman et al., 2022)	32.0	87.7	61.0	55.8	68.1	69.3	76.8	71.5	77.6	42.0	59.3	63.7
ZSCL (Zheng et al., 2023)	28.2	88.6	66.5	53.5	56.3	73.4	83.1	56.4	82.4	57.5	62.9	64.4
MoE-Adapter (Yu et al., 2024)	30.0	89.6	**73.9**	58.7	69.3	79.3	**88.1**	**76.5**	89.1	65.3	**65.8**	71.4
RAIL-Primal (Xu et al., 2024)	32.9	94.5	69.9	58.1	**71.8**	**84.4**	**88.5**	70.4	89.0	**66.1**	**65.7**	71.9
CoDyRA (Lu et al., 2024)	**34.6**	**95.8**	**73.9**	**60.0**	**77.1**	81.3	86.6	75.9	**89.9**	**66.1**	65.3	**73.3**
MoRAM	**36.7**	**95.4**	**74.9**	**61.9**	**77.1**	**82.6**	85.3	**76.0**	**90.5**	**67.0**	65.6	**73.9**
Last												
LwF (Li & Hoiem, 2017)	22.1	58.2	17.9	32.1	28.1	66.7	46.0	84.3	64.1	31.5	60.1	46.5
LwF-VR (Ding et al., 2022)	22.9	89.8	59.3	57.1	57.6	79.2	78.3	77.7	83.6	60.1	69.8	66.9
WiSE-FT (Wortsman et al., 2022)	30.8	88.9	59.6	60.3	80.9	81.7	77.1	**94.9**	83.2	62.8	70.0	71.9
ZSCL (Zheng et al., 2023)	26.8	88.5	63.7	55.7	60.2	82.1	82.6	58.6	85.9	66.7	70.4	67.4
MoE-Adapter (Yu et al., 2024)	30.1	89.3	**74.9**	**64.0**	82.3	89.4	**87.1**	89.0	89.1	69.5	72.5	76.1
RAIL-Primal (Xu et al., 2024)	**32.9**	95.1	70.3	63.2	81.5	**95.6**	**88.5**	89.7	89.0	72.5	71.0	77.2
CoDyRA (Lu et al., 2024)	31.6	**95.5**	72.8	63.5	**85.0**	89.7	85.0	94.7	**93.2**	**73.6**	**73.0**	**78.0**
MoRAM	**32.5**	**95.3**	**75.3**	**66.6**	**87.8**	**92.6**	86.3	**96.3**	**92.6**	**73.5**	**73.8**	**79.3**

(Order 2), as shown in Table 17. The results align with those in Table 1, confirming that MoRAM consistently achieves state-of-the-art performance.

A.10. Computation Cost

Table 11 summarizes the per-task trainable parameters of various continual-learning methods. Standard LoRA (Hu et al., 2021), CoDyRA (Lu et al., 2024), and O-LoRA (Wang et al., 2023a) each introduce $r(d_{\text{in}}+d_{\text{out}})$ new parameters per weight matrix. Mixture-of-Experts variants such as MoE-LoRA and MoE-Adapter (Yu et al., 2024) additionally train a router module to controll the usage of each LoRA experts, inducing d_{in} additional paramters for each experts. LB-CL (Qiao & Mahdavi, 2024) introduce r additional parameters, mimic the singular values of SVD.

By contrast, MoRAM requires only $rd_{\text{in}} + kd_{\text{out}}$ activated trainable parameters per task, where $k \leq r$ is the activation budget, and the trainable parameter is at most the same as a standard LoRA. Despite the small number of parameter activated and trained, MoRAM achieves superior continual learning performance, and reaches comparable performance in general fine-tuning with only one-third of the activated parameters of a standard LoRA.

Trainable parameters and training GPU memory. Beyond the estimated parameter counts in Table 11, in Table 18, we measured the actual trainable parameters for each continual-learning task and GPU memory usage, under the same settings as Table 1 in the main paper.

LWF (Li & Hoiem, 2017) and ZSCL (Zheng et al., 2023) perform full-parameter fine-tuning, consuming the most parameters and memory. MoE-Adapters (Yu et al., 2024) maintains a router with 22 rank-64 adapter experts (top-2 activated) and a DDAS domain predictor. CoDyRA (Lu et al., 2024) trains a single rank-16 LoRA per task, reducing its footprint to 4.4 M parameters. MoRAM introduces 16 rank-1 experts per task, with no additional router, for a total of 4.4 M trainable parameters and keeps a low gpu memory usage, thanks to our novel self-activated sparse mixture of ranks design.

Analysis of post-pruning. While this approach entails linear storage growth, our atomic structure offers a distinct advantage over conventional LoRA. Unlike standard matrices that require complex post-hoc decomposition (e.g., SVD) to compress, our rank-1 experts are independent and can be

Table 13. Overall results on the SuperNI Benchmark using the T5-Large backbone. We report Average Performance (AP, ↑) and Forgetting (FT, ↓). The best results for the stability-plasticity trade-off are highlighted in bold for methods with and without memory replay, respectively.

Methods	Replay	SuperNI	
		AP	FT
Replay-Based Methods			
Replay	✓	35.37	16.92
SAPT	✓	51.54	0.91
MoRAM	✓	**51.79**	**0.73**
Replay-Free Methods			
L2P	✗	15.18	3.65
IncLoRA	✗	12.33	41.93
C-LoRA	✗	22.69	24.25
O-LoRA	✗	26.37	19.15
MoRAM	✗	**39.62**	**5.74**

Table 14. Order Robustness Analysis on standard CL benchmark with T5-Large. We report the accuracy for each order and the average accuracy ± the standard deviation.

Method	Order 1	Order 2	Order 3	Avg ± Std
SeqFT	18.9	24.9	41.7	28.5 ± 11.82
L2P	60.3	61.7	61.1	61.0 ± 0.70
LFPT5	67.6	72.6	77.9	72.7 ± 5.15
O-LoRA	75.4	75.7	76.3	75.8 ± 0.46
MoRAM	**77.4**	**77.5**	**77.9**	**77.6 ± 0.26**

individually assessed. Consequently, the model inherently supports post-pruning, retaining only atoms that exceed a cumulative activation threshold, allowing for storage reduction with minimal performance degradation if required.

We probe the effects of pruning in Table 19, where we collect the cumulative activation mass of all rank-1 memories during training and retain only the subset required to capture the top 99% of the total activation mass, which on average prunes approximately 30% of the parameter storage. We find that the degradation to performance is minimal, confirming that the model naturally learns a sparse representation where information is concentrated in a concise set of high-utility rank-1 memories.

A.11. Extended Visualizations of Aggregated Rank Activations

To complement the qualitative examples in Fig. 3, we include a statistical aggregation of rank-1 expert utilization over the entire test set for each task. This heatmap (Fig. 5) provides a global view of the routing behavior and confirms that the patterns observed in Fig. 3 are representative of the model's overall dynamics. The heatmap (Fig. 5) visualizes

Table 15. Performance comparison on the HumanEval benchmark, reported in terms of Pass@1, Pass@5, and Pass@10.

HumanEval	Pass@1	Pass@5	Pass@10
LoRI-D	43.2	57.6	63.2
LoRI-S	41.3	54.4	59.6
MoRAM	**47.6**	**60.9**	**70.1**

the activation ratio of each rank-1 expert (x-axis) across three scenarios (y-axis) in Fig. 3:

1. Task 1 Data (after Task 1): Consistent with the qualitative results in Fig. 3a, we observe statistically dominant usage of Rank 0 (airplane semantics) and Rank 11 (background/sky). Rank 11 shows higher overall activation frequency as it captures common background tokens, which constitute a larger portion of image patches than the object itself.

2. Task 1 Data (after Task 2): Crucially, the activation pattern remains virtually unchanged after training on Task 2. The heatmap shows near-zero activation for the newly introduced Task 2 experts (Ranks 16-31). This statistically proves that our routing mechanism is stable: "old" data does not drift to "new" experts, effectively preventing catastrophic forgetting.

3. Task 2 Data (after Task 2): We observe a distinct, dual-mode behavior:

   (a) Knowledge Reuse: Old Rank 11 is reactivated, confirming that the model reuses the generic "blue sky" feature for the new task.

   (b) High Diversity: Unlike the concentrated pattern of Task 1 (Aircraft with homogeneous airplane images), Task 2 (Caltech101 with 101 diverse categories) utilizes a broad spectrum of new experts (e.g., Ranks 20, 24, 29, 30). This aligns with our design goal: fine-grained experts allow the model to dedicate different subspaces to the highly diverse semantics of the new task.

We explicitly chose to visualize activations at specific representative layers rather than averaging across the entire depth of the model. In the morden deep models, different layers specialize in distinct feature types (e.g., low-level textures vs. high-level semantics). Averaging expert usage across all layers would smooth out these distinct signatures and obscure the specialized routing behavior we aim to demonstrate.

A.12. Extended Visualizations of Rank Activations

In Sec.4.2 (Fig.3), we illustrated rank activations during the learning of Task 1 and Task 2. Here, we extend these

Table 16. Comparison to InfLoRA and performance robustness. We report mean and standard deviation across 3 independent runs. Best performances are marked in **bold**.

Method	Cars	Aircraft	OxfordPet	Food	SUN397	MNIST	Flowers	DTD	Caltech101	EuroSAT	*Average*
Transfer											
InfLoRA	–	$72.26^{\pm 0.56}$	$36.19^{\pm 0.64}$	$38.46^{\pm 0.39}$	$55.22^{\pm 1.65}$	$73.19^{\pm 0.55}$	$39.32^{\pm 1.54}$	$80.29^{\pm 0.91}$	$51.19^{\pm 1.16}$	$55.05^{\pm 0.51}$	$55.69^{\pm 0.24}$
CoDyRA	–	$74.3^{\pm 0.52}$	$36.8^{\pm 0.23}$	$44.2^{\pm 0.56}$	$\mathbf{69.9^{\pm 0.56}}$	$\mathbf{83.5^{\pm 0.23}}$	$42.8^{\pm 0.18}$	$\mathbf{88.9^{\pm 0.42}}$	$64.6^{\pm 0.47}$	$\mathbf{63.4^{\pm 0.56}}$	$63.2^{\pm 0.28}$
MoRAM	–	$\mathbf{74.5^{\pm 0.51}}$	$\mathbf{38.1^{\pm 0.24}}$	$\mathbf{46.9^{\pm 0.56}}$	$65.3^{\pm 0.44}$	$82.9^{\pm 0.18}$	$\mathbf{45.8^{\pm 0.31}}$	$88.2^{\pm 0.15}$	$\mathbf{65.1^{\pm 0.35}}$	$62.9^{\pm 0.10}$	$\mathbf{63.3^{\pm 0.26}}$
Average											
InfLoRA	$20.49^{\pm 0.98}$	$78.58^{\pm 1.02}$	$48.5^{\pm 1.18}$	$66.59^{\pm 1.51}$	$71.83^{\pm 0.80}$	$76.79^{\pm 0.34}$	$61.45^{\pm 1.36}$	$82.59^{\pm 0.86}$	$55.3^{\pm 1.34}$	$56.67^{\pm 0.59}$	$62.48^{\pm 0.31}$
CoDyRA	$41.4^{\pm 0.28}$	$81^{\pm 0.38}$	$58.7^{\pm 0.26}$	$77.8^{\pm 0.47}$	$83.4^{\pm 0.39}$	$\mathbf{84.6^{\pm 0.28}}$	$64.5^{\pm 0.14}$	$\mathbf{90.4^{\pm 0.40}}$	$67.2^{\pm 0.23}$	$\mathbf{64.4^{\pm 0.47}}$	$71.3^{\pm 0.18}$
MoRAM	$\mathbf{44.1^{\pm 0.24}}$	$\mathbf{81.6^{\pm 0.34}}$	$\mathbf{64.6^{\pm 0.34}}$	$\mathbf{79.6^{\pm 0.37}}$	$\mathbf{83.9^{\pm 0.36}}$	$84.4^{\pm 0.15}$	$\mathbf{66.5^{\pm 0.24}}$	$89.7^{\pm 0.07}$	$\mathbf{68.4^{\pm 0.38}}$	$64.1^{\pm 0.09}$	$\mathbf{72.7^{\pm 0.17}}$
Last											
InfLoRA	$18.26^{\pm 0.49}$	$\mathbf{82.36^{\pm 0.92}}$	$46.57^{\pm 0.89}$	$79.38^{\pm 2.22}$	$76.16^{\pm 1.61}$	$79.58^{\pm 0.60}$	$95.74^{\pm 0.44}$	$87.78^{\pm 0.85}$	$71.11^{\pm 0.73}$	$73.05^{\pm 0.19}$	$70.99^{\pm 0.24}$
CoDyRA	$\mathbf{37.7^{\pm 0.42}}$	$81.5^{\pm 0.24}$	$65.1^{\pm 0.63}$	$89.9^{\pm 0.55}$	$91.4^{\pm 0.38}$	$85.5^{\pm 0.16}$	$96.8^{\pm 0.08}$	$\mathbf{93.3^{\pm 0.30}}$	$77.3^{\pm 0.66}$	$73.5^{\pm 0.21}$	$79.2^{\pm 0.18}$
MoRAM	$\mathbf{37.7^{\pm 0.28}}$	$81.5^{\pm 0.22}$	$\mathbf{70.7^{\pm 0.49}}$	$\mathbf{92.4^{\pm 0.20}}$	$\mathbf{95^{\pm 0.34}}$	$\mathbf{86^{\pm 0.13}}$	$\mathbf{97.6^{\pm 0.19}}$	$92.6^{\pm 0.10}$	$\mathbf{81^{\pm 0.35}}$	$\mathbf{74.7^{\pm 0.06}}$	$\mathbf{80.9^{\pm 0.12}}$

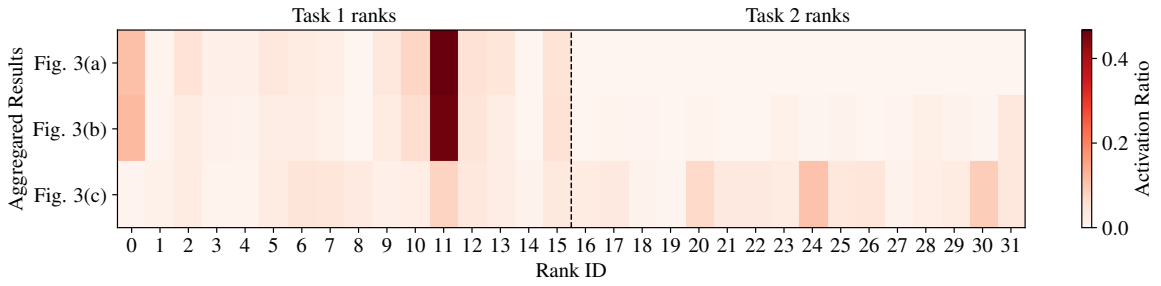

Figure 5. Averaged activation ratio of each rank-1 expert across three scenarios in Fig. 3

visualizations to additional tasks and scenarios in Fig.6 and Fig.7.

MoRAM retains task-specific semantics without forgetting. Fig. 6 shows the activation maps for the same Task 1 image after training on Task 1 (a), Task 2 (b), and the last Task 10 (c). Patches corresponding to the airplane object are outlined in orange. In all three snapshots, Rank at index 0 remains consistently and exclusively activated for those airplane patches, demonstrating that MoRAM has effectively memorized the airplane-specific knowledge into Rank 0. Even after 10 subsequent tasks, this pattern remains unchanged, indicating that later updates do not overwrite or interfere with the learned airplane representations. In other words, MoRAM effectively memorizes and preserves task-relevant semantics, thereby mitigating catastrophic forgetting.

MoRAM encodes generic semantics that are reused across tasks. Fig. 7 examines an input image from Task 9 before and after learning Task 9. Panel (a) shows the activation map of data from Task 1 after learning Task 1: Rank 11 (outlined in blue) already responds strongly to sky-background patches, demonstrating that MoRAM has stored a generic "blue sky" concept in this rank. In panel (b), when we infer on the Task 9 image before training on Task 9, Rank 11 is again activated for the sky regions, confirming that MoRAM reuses this shared knowledge for unseen data. Finally, panel (c) shows the activation map after learning Task 9: Rank 11 remains dedicated to the sky background, while newly initialized ranks specialize in the "car" object semantics. This persistent reuse of Rank 11 across tasks illustrates MoRAM 's ability to capture and retain common features as reusable memory slots, reducing redundancy and facilitating knowledge reuse.

A.13. Statistical Analyses of Contributing Rank Activations

Fig. 8 and Fig. 9 plot the cumulative sum of averaged rank activations after training on all tasks, sorted in descending order, for several representative layers and locations within pre-trained models. The red dashed line marks the point at which 99% of the total activation mass is reached, allowing us to quantify how many ranks are truly contributing to the model's adaptation. Two key observations emerge:

1. Sparse Mixture: only a small subset of ranks is needed. Across all layers and positions, we find that fewer than 10% of the total ranks suffice to capture 99% of the activations. This highlights the extreme sparsity of MoRAM 's self-activated mixture: most ranks remain dormant for any given input, while a compact set of highly relevant ranks drives

Table 17. Comparisons on X-TAIL (Order 2) for each domain in terms of "Transfer", "Average", and "Last" scores (%).

Method	Cars	Aircraft	OxfordPet	Food	SUN397	MNIST	Flowers	DTD	Caltech101	EuroSAT	*Average*
CLIP											
Zero-shot	66.1	23.5	86.7	84	63.7	46.7	63.6	37.3	76.8	36.7	58.5
Transfer											
Zero-shot (Radford et al., 2021)	–	**23.5**	86.7	84	**63.7**	46.7	63.6	37.3	76.8	36.7	57.7
LwF (Li & Hoiem, 2017)	–	20.0	74.1	79.6	58.1	34.1	48.9	27.7	64.4	15.1	46.9
WiSE-FT (Wortsman et al., 2022)	–	21.3	79.5	83.3	61.0	39.9	56.5	29.6	68.0	20.8	51.1
ZSCL (Zheng et al., 2023)	–	23.0	84.3	**87.2**	**63.0**	42.1	65.2	34.6	71.4	**40.9**	56.9
MoE-Adapter (Yu et al., 2024)	–	17.1	87.2	**87.5**	58.4	12.6	65.5	35.9	70.0	17.9	50.2
RAIL-Primal (Xu et al., 2024)	–	**23.5**	86.7	84	**63.7**	46.7	63.6	37.3	76.8	36.7	57.7
CoDyRA (Lu et al., 2024)	–	**23.6**	**89.2**	83	62	**51**	**71.4**	**38**	**77.4**	**39**	**59.4**
MoRAM	–	**23.6**	**88.7**	83.4	62.6	**51.2**	**69.9**	**39.3**	**77.5**	**39**	**59.5**
Average											
LwF (Li & Hoiem, 2017)	49.0	27.4	69.7	83.0	65.7	42.2	63.5	33.1	68.5	17.5	52.0
WiSE-FT (Wortsman et al., 2022)	57.9	29.6	77.8	85.4	68.0	51.6	69.3	35.5	71.0	23.0	56.9
ZSCL (Zheng et al., 2023)	74.4	36.4	86.7	**88.7**	68.9	50.0	75.1	40.1	72.5	43.7	63.6
MoE-Adapter (Yu et al., 2024)	74.4	38.6	**87.7**	**87.3**	67.9	50.6	76.5	43.7	72.3	18.8	61.8
RAIL-Primal (Xu et al., 2024)	77.9	**40.4**	85.6	83.3	68.3	62.2	76.6	45.8	**80.4**	41.7	66.2
CoDyRA (Lu et al., 2024)	**80**	39.2	**92.5**	85.2	**69.2**	**73.7**	**79.6**	**46.2**	**78.6**	**44.1**	**68.8**
MoRAM	**80.2**	**40.1**	**92.5**	84.7	**70.1**	**74**	**80.1**	**48.7**	78.4	**44.4**	**69.3**
Last											
LwF (Li & Hoiem, 2017)	29.6	17.5	63.0	83.8	67.7	44.9	79.3	44.8	**84.6**	39.0	55.4
WiSE-FT (Wortsman et al., 2022)	46.1	23.5	71.3	85.7	70.2	59.1	85.5	47.9	82.4	42.8	61.5
ZSCL (Zheng et al., 2023)	71.7	35.3	86.5	**89.2**	71.8	52.3	89.8	52.0	77.1	68.4	69.4
MoE-Adapter (Yu et al., 2024)	75.1	**41.1**	87.9	**87.1**	74.1	89.7	92.6	61.2	81.0	27.4	71.7
RAIL-Primal (Xu et al., 2024)	77.7	**41.9**	86.1	83.3	71.8	91.6	**97.3**	**66.4**	**94.8**	86.9	**79.8**
CoDyRA (Lu et al., 2024)	**79**	38.6	**92.6**	86.4	**74.7**	**95.2**	93	64.7	81.9	**92.2**	**79.8**
MoRAM	**79.3**	38.9	**93.1**	85.4	**74.9**	**96.4**	**94.1**	**69.9**	82	**92.9**	**80.7**

Table 18. Trainable parameters and averaged training GPU memory per task.

Method	**Trainable Params. (Million)**	**GPU Mem. (MiB)**
LWF (Li & Hoiem, 2017)	129.6	32172
ZSCL (Zheng et al., 2023)	129.6	26290
MoE-Adapters (Yu et al., 2024)	59.8	22358
CoDyRA (Lu et al., 2024)	4.4	21770
MoRAM	4.4	21090

the adaptation.

2. Adaptive Activation: The number of ranks required varies by layers and modules. The number of ranks needed to capture 99% of the cumulative activation mass varies across both layer depth and module type. For example, in Fig. 8, the MLP's output projection (`c-proj`) in Layer 1 of the vision encoder requires 16 ranks, whereas the same module in Layer 1 of the text encoder needs only 3 ranks.

To provide a broader view, Fig. 10 shows the required rank counts for every module in the pre-trained model. We observe that most attention modules requires around 6–12 ranks, while the second MLP projection generally demands more ranks in early layers, peaking in the first few blocks, and then steadily declines in deeper layers.

Coupling the rank activation budget with rank pruning, MoRAM adapts the number of ranks needed to activate at each layer and module. This adaptive sparsity maximizes the efficient use of newly acquired knowledge during continual learning.

Table 19. Analysis of post-pruning. After training of each task, we retain the subset required to capture the top 99% of the total activation.

Method	Cars	Aircraft	OxfordPet	Food	SUN397	MNIST	Flowers	DTD	Caltech101	EuroSAT	*Average*
Transfer											
MoRAM	–	74.5	38.1	46.9	65.3	82.9	45.8	88.2	65.1	62.9	63.3
MoRAM *w/* pruning	–	75.1	38.0	43.6	68.4	83.9	48.0	88.8	65.3	62.3	63.7
Average											
MoRAM	44.1	81.6	64.6	79.6	83.9	84.4	66.5	89.7	68.4	64.1	72.7
MoRAM *w/* pruning	42.3	81.0	62.9	75.4	82.7	83.2	66.3	89.6	67.6	63.0	71.4
Last											
MoRAM	37.7	81.5	70.7	92.4	95.0	86.0	97.6	92.6	81.0	74.7	80.9
MoRAM *w/* pruning	34.6	80.8	67.9	89.4	94.2	85.3	97.3	92.6	79.8	73.7	79.5

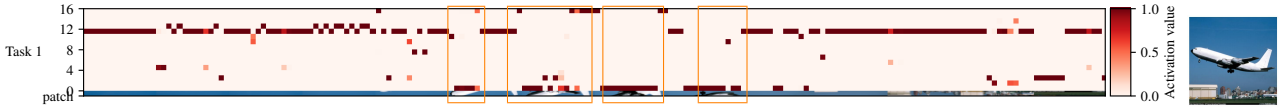

(a) Rank Activations of MoRAM on data from Task 1 after learning Task 1.

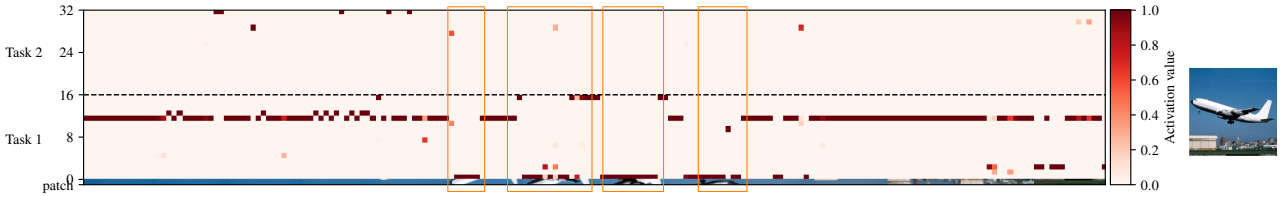

(b) Rank Activations of MoRAM on data from Task 1 after learning Task 2.

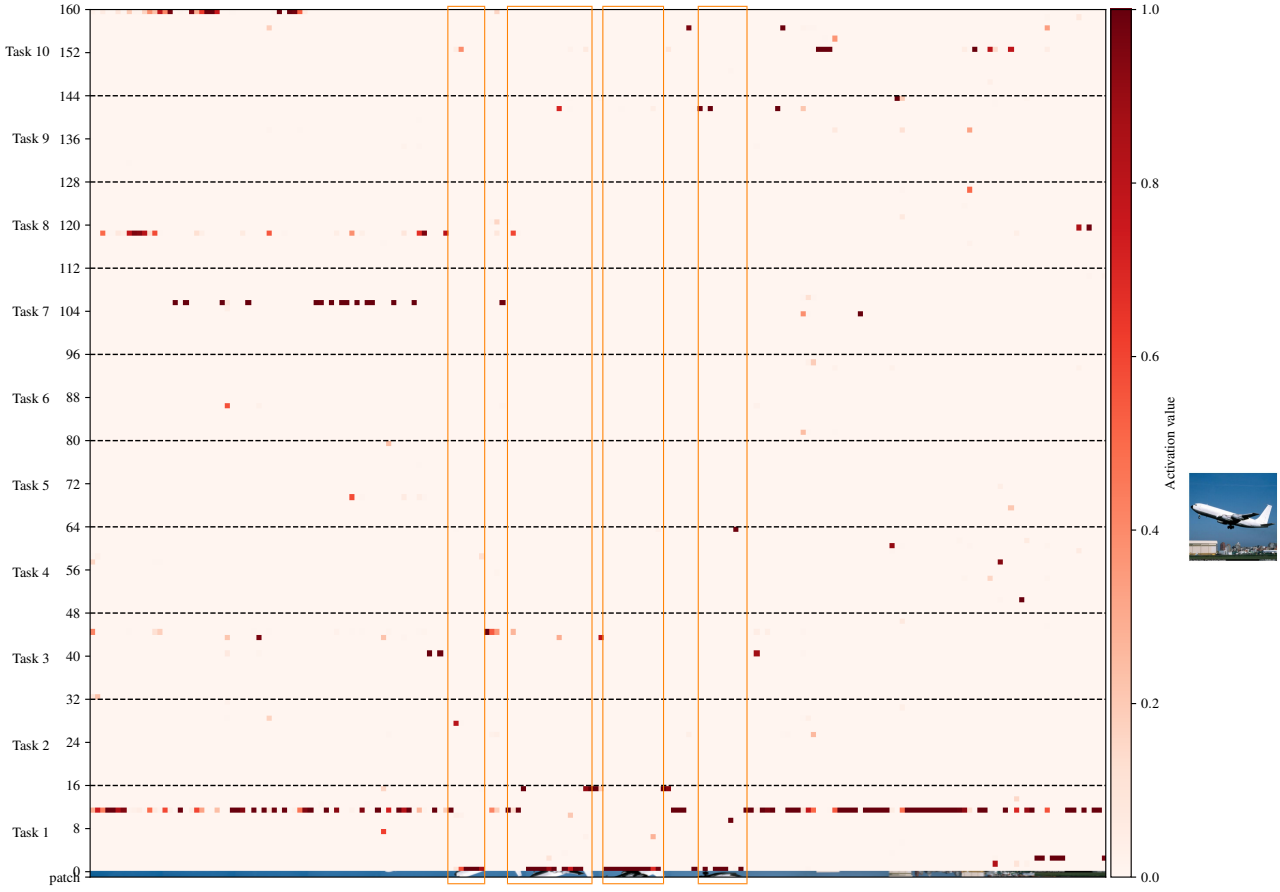

(c) Rank Activations of MoRAM on data from Task 1 after learning Task 10.

Figure 6. Extended view of Fig. 3 illustrating **forgetting mitigation**. Regions corresponding to object semantics are highlighted with orange bounding boxes. Zoom in for details.

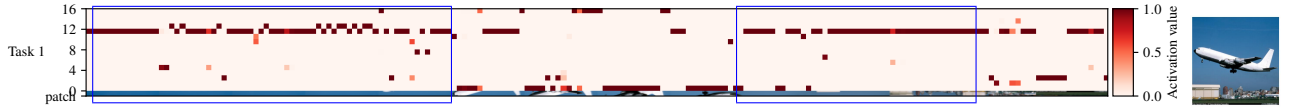

(a) Rank Activations of MoRAM on data from Task 1 after learning Task 1.

(b) Rank Activations of MoRAM on data from Task 9 after learning Task 1.

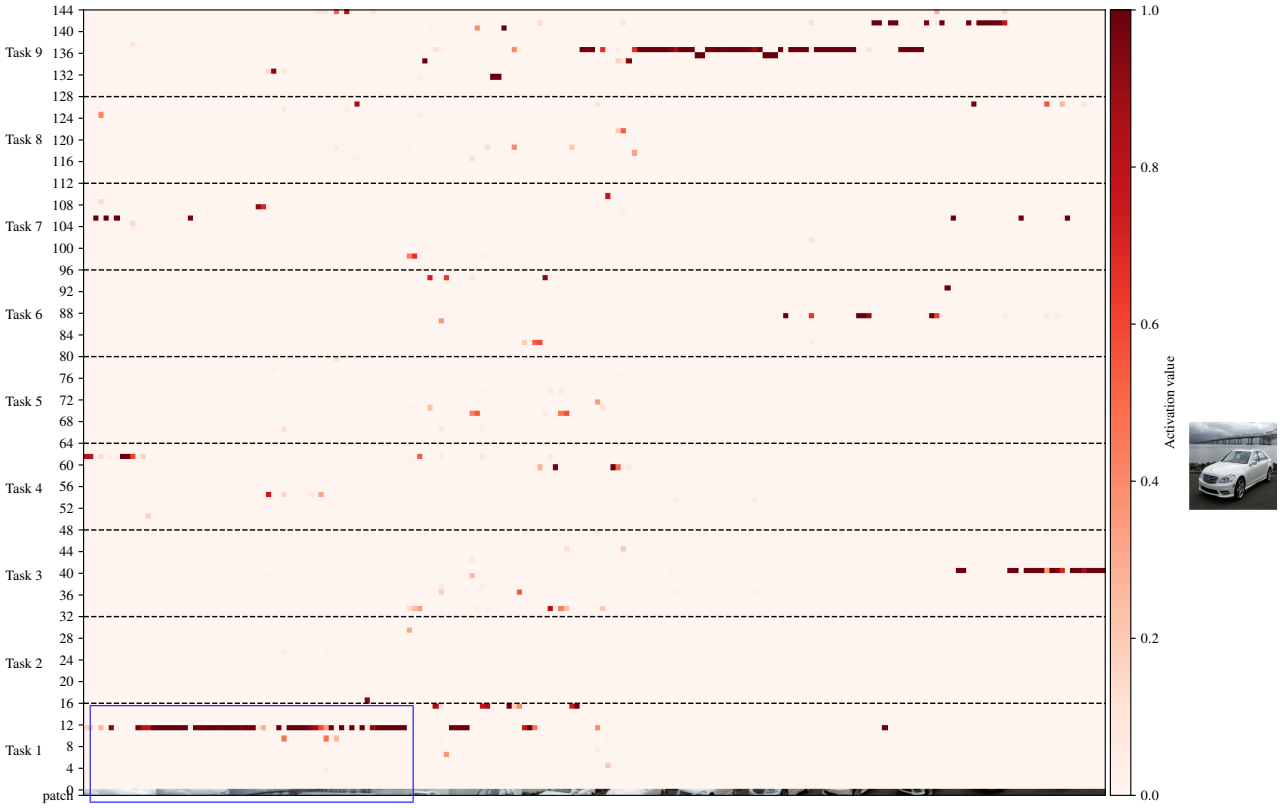

(c) Rank Activations of MoRAM on data from Task 9 after learning Task 9.

Figure 7. Extended view of Fig. 3 illustrating **knowledge reuse**. Regions corresponding to generic input tokens (*e.g.* blue sky) are highlighted with blue bounding boxes. Zoom in for details.

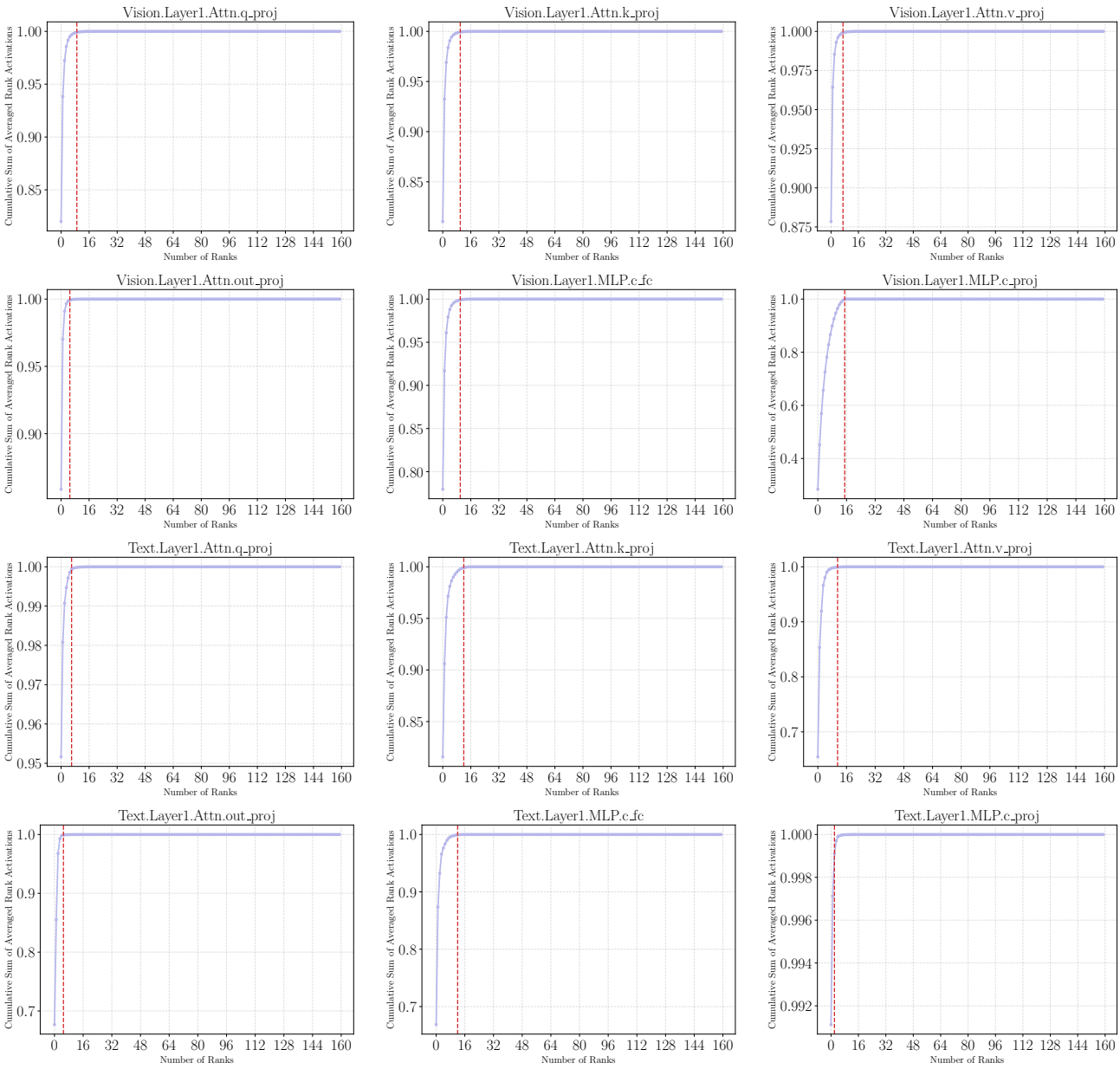

Figure 8. Statistical analyses on the number of ranks required to capture 99% of cumulative sum (indicated in red dashed line) of all rank activations. Activations were gathered from the model after training on all tasks, and results are shown for a representative selection of layers and positions within the pre-trained model.

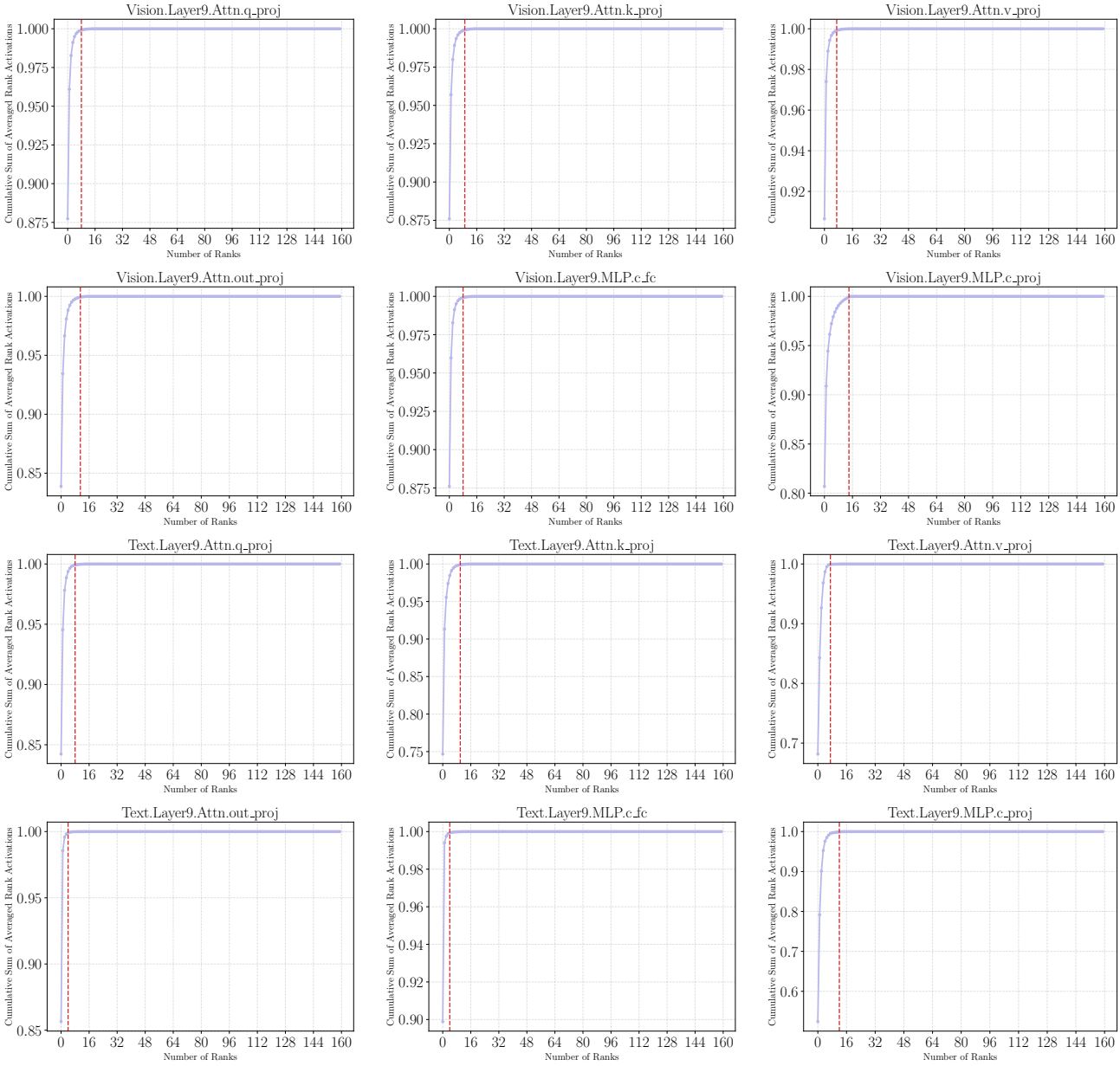

Figure 9. Statistical analyses on the number of ranks required to capture 99% of cumulative sum (indicated in red dashed line) of all rank activations. Activations were gathered from the model after training on all tasks, and results are shown for a representative selection of layers and positions within the pre-trained model.

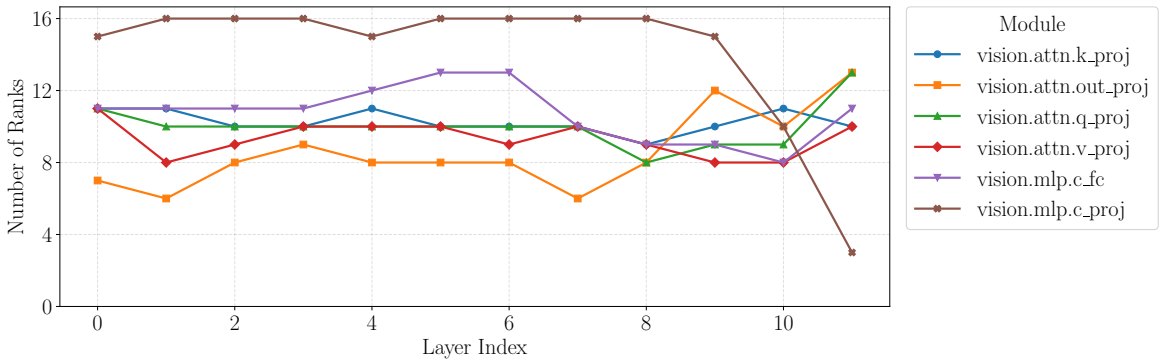

(a) Vision Encoder

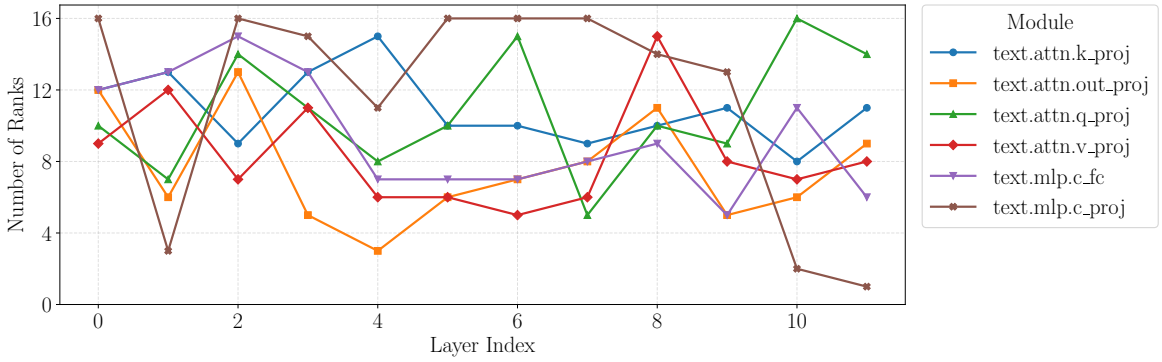

(b) Text Encoder

Figure 10. Required ranks to capture 99 % of cumulative activations, shown across different pre-trained model layers and projection locations.